Cell Reports

Resource

Host genetics highlights IFN-γ-dependent *Toxoplasma* genes encoding secreted and non-secreted virulence factors in *in vivo* CRISPR screens

Graphical abstract

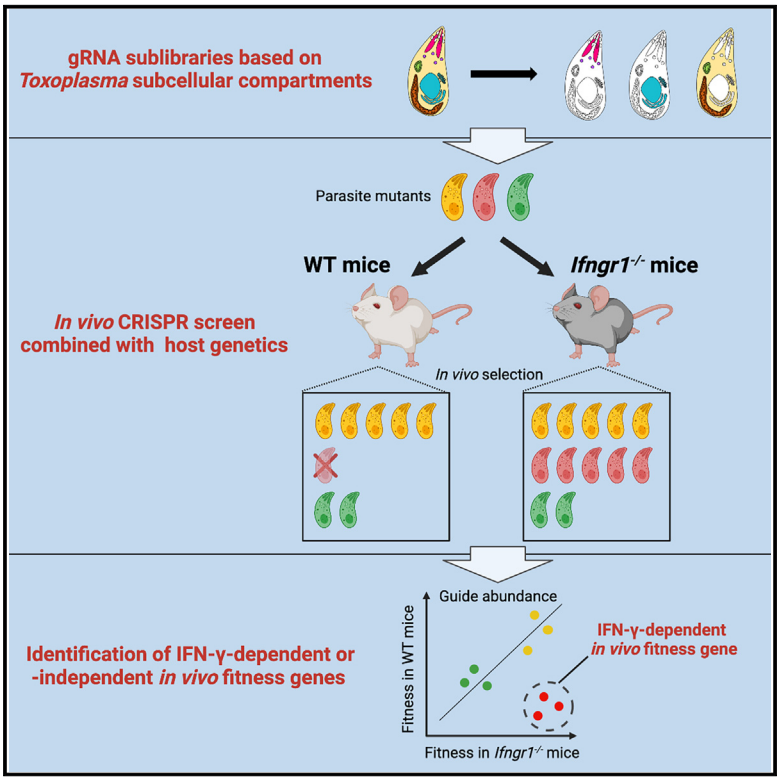

Highlights

- Host genetics is combined with highly reproducible *Toxoplasma in vivo* CRISPR screen
- The *in vivo* CRISPR screen identifies secreted and non-secreted virulence factors
- GRA72 is involved in correct GRA17/GRA23 localization and PV maintenance
- *Toxoplasma* UFMylation-related genes are involved in IFN-γ-dependent virulence

Authors

Yuta Tachibana, Emi Hashizaki, Miwa Sasai, Masahiro Yamamoto

Correspondence

myamamoto@biken.osaka-u.ac.jp

In brief

Toxoplasma may exploit numerous virulence factors to fit *in vivo* in immune-competent hosts, although most of them remain unidentified. Tachibana et al. utilize immune gene-knockout mice for *in vivo* CRISPR screen and demonstrate that host genetics can be combined with microbe genetics to explore the immune-related virulence factors.

Tachibana et al., 2023, Cell Reports *42*, 112592
June 27, 2023
https://doi.org/10.1016/j.celrep.2023.112592

CellPress

Cell Reports

CellPress
OPEN ACCESS

Resource

Host genetics highlights IFN-γ-dependent *Toxoplasma* genes encoding secreted and non-secreted virulence factors in *in vivo* CRISPR screens

Yuta Tachibana,[1,2] Emi Hashizaki,[1,2] Miwa Sasai,[1,2,3] and Masahiro Yamamoto[1,2,3,4,*]
[1]Department of Immunoparasitology, Research Institute for Microbial Diseases, Osaka University, Suita, Osaka, Japan
[2]Laboratory of Immunoparasitology, WPI Immunology Frontier Research Center, Osaka University, Suita, Osaka, Japan
[3]Department of Immunoparasitology, Center for Infectious Disease Education and Research, Osaka University, Suita, Osaka 565-0871, Japan
[4]Lead contact
*Correspondence: myamamoto@biken.osaka-u.ac.jp
https://doi.org/10.1016/j.celrep.2023.112592

SUMMARY

Secreted virulence factors of *Toxoplasma* to survive in immune-competent hosts have been extensively explored by classical genetics and *in vivo* CRISPR screen methods, whereas their requirements in immune-deficient hosts are incompletely understood. Those of non-secreted virulence factors are further enigmatic. Here we develop an *in vivo* CRISPR screen system to enrich not only secreted but also non-secreted virulence factors in virulent *Toxoplasma*-infected C57BL/6 mice. Notably, combined usage of immune-deficient *Ifngr1*$^{-/-}$ mice highlights genes encoding various non-secreted proteins as well as well-known effectors such as ROP5, ROP18, GRA12, and GRA45 as interferon-γ (IFN-γ)-dependent virulence genes. The screen results suggest a role of GRA72 for normal GRA17/GRA23 localization and the IFN-γ-dependent role of UFMylation-related genes. Collectively, our study demonstrates that host genetics can complement *in vivo* CRISPR screens to highlight genes encoding IFN-γ-dependent secreted and non-secreted virulence factors in *Toxoplasma*.

INTRODUCTION

Toxoplasma is an important protozoan pathogen that can cause life-threatening toxoplasmosis in humans and animals.[1,2] To date, most of the *Toxoplasma* virulence genes have been identified through classical forward and reverse genetics methods. The forward genetics identified several virulence genes such as ROP5, ROP16, and ROP18,[3–6] which are family members of rhoptry bulb proteins (ROPs) secreted into host cells during *Toxoplasma* infection.[7,8] Those ROPs suppress host immunity and thus contribute to the parasite *in vivo* fitness.[9–14] Although forward genetics is a powerful strategy, the method relies on polymorphisms in the virulence genes. The classical reverse genetics using individual gene-knockout *Toxoplasma* is solid; however, the gene of interest is intentionally selected. It also remains unclear whether the gene is involved in virulence.

The *in vitro* CRISPR screen method using the genome-wide guide RNA (gRNA) library has been recently developed to identify *in vitro* fitness genes that are essential for *Toxoplasma* proliferation in human foreskin fibroblasts (HFFs).[15] Subsequently, three studies have applied the method in mice, advancing our understanding of *Toxoplasma in vivo* fitness genes.[16–18] These *in vivo* CRISPR screens utilized small-scale gRNA sublibraries mainly targeting ROPs and dense granule proteins (GRAs) (hereafter termed ROP/GRA) and identified several virulence factors.[16–18] However, genes predicted to encode ROP/GRA are only ~3% of the total 8,100 *Toxoplasma* genes. Thus, it remains unclear which *Toxoplasma* genes other than ROP/GRA (non-ROP/GRA genes) are required for the parasite *in vivo* fitness.

In general, not only pathogen genes but also host impediments called bottlenecks, such as host immunity and nutritional limitations, influence pathogen *in vivo* fitness and virulence.[19] The host immune system rapidly responds to *Toxoplasma* infection and produces interferon-γ (IFN-γ).[20,21] IFN-γ stimulation leads to robust expression of IFN-inducible effectors such as IFN-inducible guanosine triphosphatases (GTPases) to suppress the parasite proliferation.[22,23] Mice treated with anti-IFN-γ antibody or with IFN-γ gene inactivation are highly susceptible to less-virulent type II *Toxoplasma*,[24,25] demonstrating IFN-γ-dependent host immunity as an important biological bottleneck that profoundly influences the parasite *in vivo* fitness. Among ROP/GRA, ROP5, ROP18, GRA12, GRA45, and TgIST are well known to affect the parasite *in vivo* fitness in a manner dependent on IFN-γ.[26–34] However, it is poorly understood which of the other ROP/GRA genes as well as non-ROP/GRA genes contribute to IFN-γ-dependent *in vivo* fitness.

Here we have newly established a highly reproducible *in vivo* CRISPR screen system targeting both ROP/GRA and non-ROP/GRA genes using C57BL/6 mice and the virulent type I *Toxoplasma* RH strain. Strikingly, not only known ROP/GRA

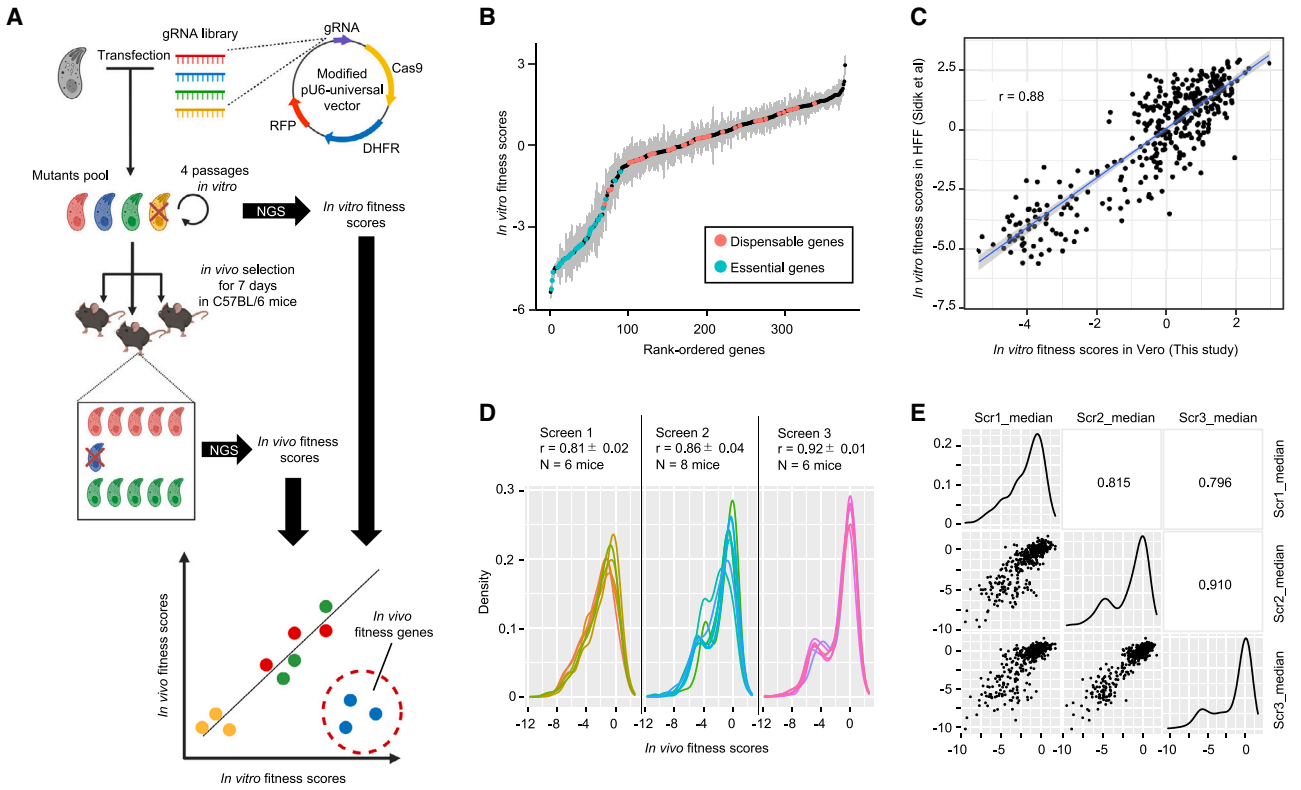

Figure 1. Highly reproducible *in vivo* CRISPR screen in virulent *Toxoplasma*

(A) Schematic of *in vivo* CRISPR screen.

(B) Rank-ordered plots for *in vitro* fitness scores of third passage. Essential and dispensable control genes are marked in cyan and coral red, respectively. Error bars (gray) represent SEM.

(C) Correlation between our *in vitro* fitness scores (third passage in Vero cells) and the *in vitro* fitness scores in HFFs.

(D) Overlay of *in vivo* fitness scores for each of WT mouse replicates from three independent screens (n = 6, 8, and 6 mice, respectively). Pearson's correlation coefficients are shown as mean ± SD.

(E) Correlations between three independent screens (Scr1, Scr2, and Scr3). Scatterplots and density plots for the median *in vivo* fitness scores are shown. Pearson's correlation coefficients are shown (upper right).

See also Figure S1.

genes but also various unreported non-ROP/GRA genes are identified as IFN-γ-dependent or -independent *in vivo* fitness genes by comparison of screen results using immune-competent wild-type (WT) and immune-deficient (*Ifngr1*$^{-/-}$) mice. The current study provides the community with a genetic resource to investigate the role of *Toxoplasma* IFN-γ-dependent and -independent *in vivo* fitness genes.

RESULTS

Highly reproducible *in vivo* CRISPR screens in C57BL/6 mice locally infected with virulent *Toxoplasma*

We designed a CRISPR screen system and generated the modified pU6-Universal vector by cloning a ribosomal skip peptide (T2A), dihydrofolate reductase (DHFR) drug selection marker, T2A, and red fluorescent protein (RFP) in frame with Cas9, where the expression of gRNA and Cas9-T2A-DHFR-T2A-RFP cassettes was independently transcribed (Figure 1A). We selected gRNAs for the genes encoding proteins predicted to localize in rhoptries and dense granules by hyperLOPIT, which is the spatial proteomics data of *Toxoplasma* tachyzoite.[35] Thus we assembled a small library (hereafter called the rhoptry/dense granule [DG] sublibrary) (Figure S1A; Tables S1A and S1B), which consisted of 3,757 gRNAs targeting 376 putative or known ROP/GRA and also rhoptry neck protein (RON) genes together with dispensable and essential control genes.[15] RH *Toxoplasma* parasites were transfected with the plasmid pools, grown in Vero cells, and selected in the presence of pyrimethamine. Following three lytic cycles, the parasites were retrieved for genomic DNA extraction, sequencing, and calculation of *in vitro* fitness scores as described previously.[36] Rank-ordered plots of *in vitro* fitness scores clearly showed that essential control genes exhibited lower scores while dispensable control genes did not (Figure 1B). Furthermore, the correlation between our *in vitro* fitness scores and the previously determined scores in HFFs was high (r = 0.88) (Figure 1C),[15] highlighting the reproducibility of our *in vitro* CRISPR screens.

Next, we attempted to establish an *in vivo* CRISPR screen system (Figure 1A). We utilized immunologically uniform inbred

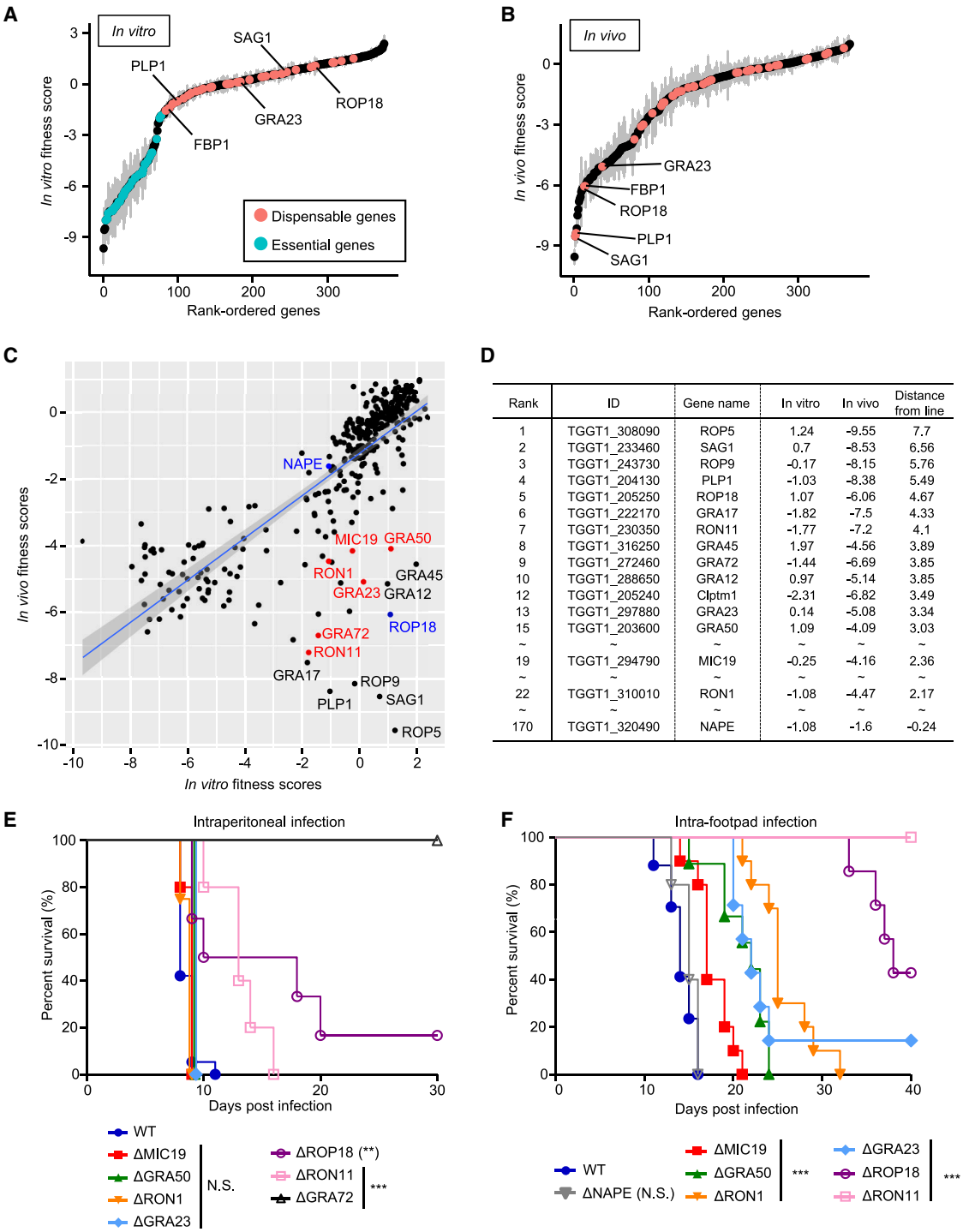

Rank	ID	Gene name	In vitro	In vivo	Distance from line
1	TGGT1_308090	ROP5	1.24	-9.55	7.7
2	TGGT1_233460	SAG1	0.7	-8.53	6.56
3	TGGT1_243730	ROP9	-0.17	-8.15	5.76
4	TGGT1_204130	PLP1	-1.03	-8.38	5.49
5	TGGT1_205250	ROP18	1.07	-6.06	4.67
6	TGGT1_222170	GRA17	-1.82	-7.5	4.33
7	TGGT1_230350	RON11	-1.77	-7.2	4.1
8	TGGT1_316250	GRA45	1.97	-4.56	3.89
9	TGGT1_272460	GRA72	-1.44	-6.69	3.85
10	TGGT1_288650	GRA12	0.97	-5.14	3.85
12	TGGT1_205240	Clptm1	-2.31	-6.82	3.49
13	TGGT1_297880	GRA23	0.14	-5.08	3.34
15	TGGT1_203600	GRA50	1.09	-4.09	3.03
~	~	~	~	~	~
19	TGGT1_294790	MIC19	-0.25	-4.16	2.36
~	~	~	~	~	~
22	TGGT1_310010	RON1	-1.08	-4.47	2.17
~	~	~	~	~	~
170	TGGT1_320490	NAPE	-1.08	-1.6	-0.24

Figure 2. *In vivo* CRISPR screen identified known and novel rhoptry/DG-related virulence genes

(A and B) Rank-ordered plots for *in vitro* fitness scores of fourth passage (A) and *in vivo* fitness scores (B). Error bars (gray) represent SEM.

(C) Scatterplot showing *in vitro* and *in vivo* fitness scores for each gene. Examples of previously reported and unreported virulence genes are labeled in black and red, respectively. ROP18 and NAPE as controls are labeled in blue.

(D) Ranking table for *in vivo* fitness genes ordered by the distance from the regression line.

(legend continued on next page)

C57BL/6 mice, the workhorses of mouse genetics. The pooled mutant parasites transfected with the rhoptry/DG sublibrary were harvested after the fourth passage in Vero cells (named the P4 sample, input for *in vivo* screen). An amount of 1×10^7 parasites per mouse, which represented coverage of ~2,600 unique gRNAs, were used for infection. According to the previous report,[16] intraperitoneal infection with this high dose of parasites in C57BL/6 mice led to death in approximately 3 days, expecting the possible experimental bottleneck due to high susceptibility. To prolong the host survival time, we tested intra-footpad infection of the 1×10^7 parasites and found that the infected mice can survive for more than 7 days (Figure S1B). At 7 days post infection, the single-cell suspension of the spleen from each mouse was retrieved and inoculated to the monolayer of Vero cells for parasite expansion, genomic DNA extraction, and sequencing (named the *in vivo* sample). *In vitro* and *in vivo* fitness scores of each gene were calculated by the definition of $\log_2$ fold change between P4 sample and the gRNA library or between each *in vivo* sample and P4 sample, respectively. To assess the reproducibility, we performed three independent *in vivo* screens. It was noteworthy that high reproducibility was observed between *in vivo* fitness scores among replicate mice ($r = 0.81–0.92$) (Figure 1D; Tables S1C and S1D). Furthermore, the median *in vivo* fitness scores among three independent screens were highly correlated ($r = 0.84 \pm 0.06$) (Figure 1E). Taken together, these results demonstrated the feasibility of highly reproducible *in vivo* CRISPR screens using C57BL/6 mice locally infected with RH *Toxoplasma*.

Comparison of CRISPR screen results with published datasets

We compared our *in vivo* CRISPR screen results with three published *in vivo* CRISPR screen datasets.[16–18] We searched for overlapping genes among four gRNA sublibraries and compared them (Figures S1C and S1D; Table S1F). It was notable that our *in vivo* fitness scores for most of the genes were well correlated with those from the previous screens ($r = 0.62–0.78$) (Figure S1D and Table S1F), suggesting the reproducibility and robustness of these screens. In addition, when we compared *in vivo* fitness scores for TgWIP (a known gene involved in parasite dissemination) between these screens, we found that TgWIP behaved similarly between them (Figure S1D), suggesting that there is no bias irrespective of infection methods (Figure S1E).

Identification of novel and known ROP/GRA *in vivo* fitness genes that affect virulence

We generated rank-ordered plots of *in vitro* and *in vivo* fitness scores of the rhoptry/DG sublibrary (Figures 2A and 2B; Table S1A). At first glance, we found that *in vivo* fitness scores of some *in vitro* dispensable control genes such as SAG1 (TGGT1_233460), PLP1 (TGGT1_204130), ROP18 (TGGT1_205250), FBP1 (TGGT1_205380), and GRA23 (TGGT1_297880) became extremely low compared with the *in vitro* scores (Figures 2A and 2B), suggesting differential behaviors of some genes in *in vitro* and *in vivo* settings. Furthermore, ROP5 (TGGT1_308090), ROP9 (TGGT1_243730), Clptm1 (TGGT1_205240), GRA17 (TGGT1_222170), GRA12 (TGGT1_288650), GRA45 (TGGT1_316250), GRA72 (TGGT1_272460), RON11 (TGGT1_230350), RON1 (TGGT1_310010), GRA50 (TGGT1_203600), and MIC19 (TGGT1_294790) had low *in vivo* fitness scores and were located distantly from the regression line (Figures 2C and 2D). Since the previously known *in vivo* fitness genes affecting virulence such as ROP5, ROP9, Clptm1, GRA17, GRA12, and GRA45 were ranked highly (Figures 2C and 2D; Table S1A),[3,4,17,28,29,37,38] these unreported *in vivo* fitness genes such as GRA72, RON11, GRA23, RON1, GRA50, and MIC19 might also affect virulence.[39–43] GRA23 and GRA50 were shown to be important for type II parasite virulence, albeit non-essential and unknown in type I parasites, respectively.[37,42,44] To test the possibility, we generated individual knockout parasites of the candidate genes using the RH *Toxoplasma* strain together with ΔROP18 or ΔNAPE parasites as positive and negative control strains, respectively (Figures 2C, 2D, S2A, and S2B). Mice were intraperitoneally infected with each knockout or WT parasites and monitored for survival (Figure 2E). All mice infected with WT, ΔMIC19, ΔGRA50, ΔRON1, or ΔGRA23 parasites similarly succumbed (Figure 2E). In sharp contrast, all mice infected with ΔGRA72 parasites survived (Figure 2E). Mice infected with ΔROP18 and ΔRON11 parasites showed significantly prolonged survival periods (Figure 2E), which was consistent with previous reports of ΔROP18 parasites.[11,45] Since our *in vivo* screen utilized the local intra-footpad infection model, parasites lacking the *in vivo* fitness genes except for GRA72 might fail to exhibit defects in virulence. It is reported that local infection likely enlarges susceptibility differences more than intraperitoneal infection at the acute phase.[46,47] Therefore, we inoculated the intra-footpad of mice with knockout parasites and monitored the survival rates (Figure 2F). Reduced virulence of ΔMIC19, ΔGRA50, ΔRON1, ΔGRA23, ΔRON11, or ΔROP18 parasites compared with WT parasites became evident in the local intra-footpad infection, while ΔNAPE parasites remained virulent (Figure 2F), thus confirming the effects of GRA23, RON1, MIC19, and GRA50 on virulence in the local infection model. Collectively, these data demonstrated that our *in vivo* CRISPR screen highlights *Toxoplasma* known and novel *in vivo* fitness genes that affect virulence.

Host IFN-γ receptor deficiency highlights known and novel IFN-γ-dependent ROP/GRA *in vivo* fitness genes

Since the *in vivo* CRISPR screen in WT mice identified *in vivo* fitness genes (Figures 1 and 2), we next asked whether all the *in vivo* fitness genes behave similarly or distinctly in mice possessing a different genotype. For instance, ΔROP5 and ΔROP18 parasites were previously reported to be less virulent in WT mice, albeit

(E) Survival curves of mice intraperitoneally infected with 10^3 tachyzoites of WT (n = 5), ΔMIC19 (n = 5), ΔGRA50 (n = 5), ΔRON1 (n = 4), ΔGRA23 (n = 4), ΔRON11 (n = 5), ΔROP18 (n = 6), and ΔGRA72 (n = 5). ***$p < 0.001$; **$p < 0.01$; N.S., not significant (log-rank test).
(F) Survival curves of mice with intra-footpad infection of 10^3 tachyzoites of WT (n = 17), ΔMIC19 (n = 10), ΔGRA50 (n = 9), ΔRON1 (n = 10), ΔGRA23 (n = 7), ΔRON11 (n = 5), ΔROP18 (n = 7), and ΔNAPE (n = 5). ***$p < 0.001$; N.S., not significant (log-rank test).
See also Figure S2.

CellPress
OPEN ACCESS

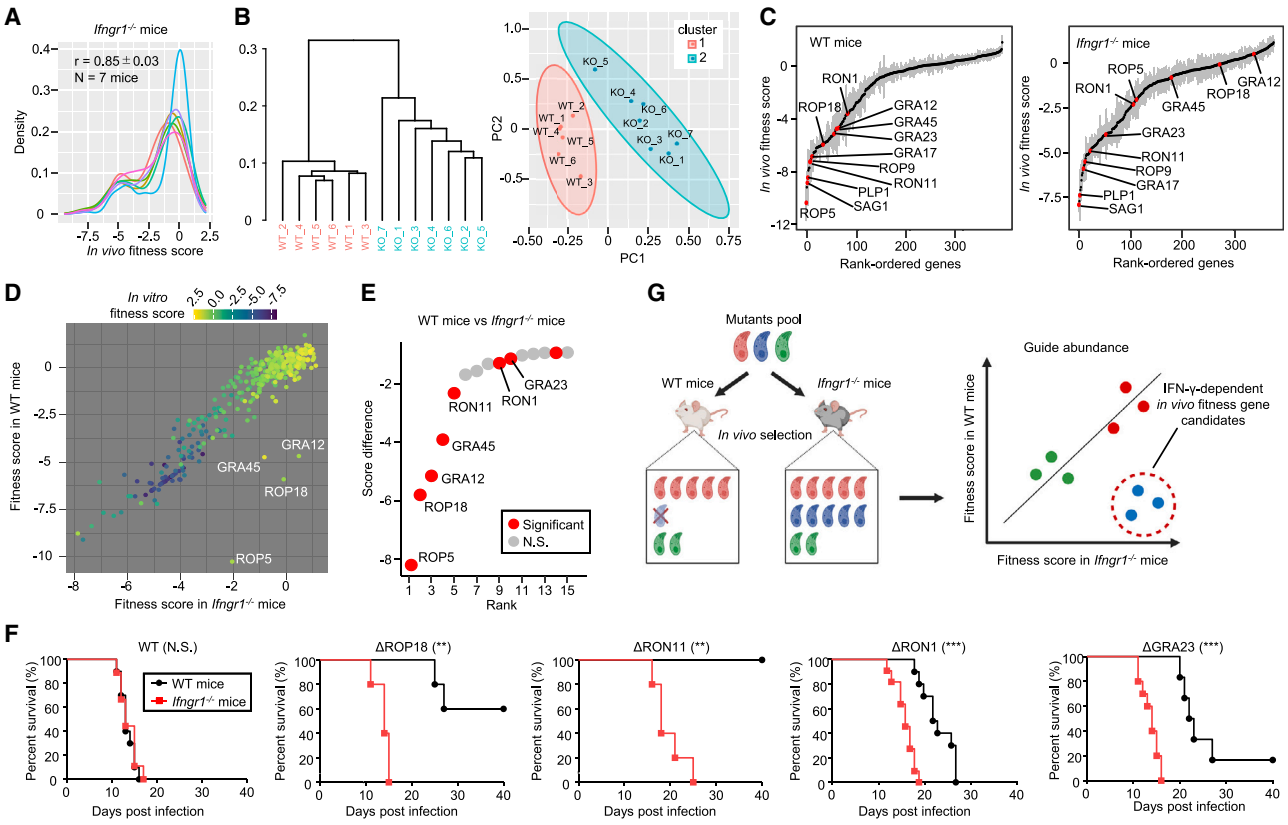

Figure 3. Host genetics combined with *in vivo* CRISPR screen revealed IFN-γ-dependent virulence genes of *Toxoplasma*

(A) Overlay of *in vivo* fitness scores for each *Ifngr1*$^{-/-}$ mouse replicates (n = 7). Pearson's correlation coefficient is shown as mean ± SD.

(B) Hierarchal clustering (left) and principal component (PC) analysis (right) for WT and *Ifngr1*$^{-/-}$ mice.

(C) Rank-ordered plots for *in vivo* fitness scores from WT or *Ifngr1*$^{-/-}$ mice. Examples of *in vivo* control genes are marked in red. Error bars (gray) represent SEM.

(D) Scatterplot showing WT and *Ifngr1*$^{-/-}$ fitness scores for each gene. Four outstanding IFN-γ-dependent fitness genes are labeled. The color of each gene indicates its *in vitro* fitness scores.

(E) The difference between WT and *Ifngr1*$^{-/-}$ mice fitness scores are calculated and ranked by the order. Plotted genes are selected with *in vitro* fitness score > −2, WT-*Ifngr1*$^{-/-}$ < −0.9, WT fitness score < −3. Significant genes ($p < 0.05$, Wilcoxon rank-sum test) are marked in red. N.S. (gray), not significant.

(F) Survival curves of WT or *Ifngr1*$^{-/-}$ mice with intra-footpad infection of 10^3 tachyzoites of the indicated mutant strains. Mouse genotype/parasite genotype (mouse numbers tested): WT/WT (n = 10), *Ifngr1*$^{-/-}$/WT (n = 9), WT/ΔRON11 (n = 5), *Ifngr1*$^{-/-}$/ΔRON11 (n = 5), WT/ΔRON1 (n = 10), *Ifngr1*$^{-/-}$/ΔRON1 (n = 11), WT/ΔGRA23 (n = 6), *Ifngr1*$^{-/-}$/ΔGRA23 (n = 10), WT/ΔROP18 (n = 5), and *Ifngr1*$^{-/-}$/ΔROP18 (n = 5). ***$p < 0.001$; **$p < 0.01$; N.S., not significant (log-rank test).

(G) Schematic of the *in vivo* CRISPR screen of *Toxoplasma* in different genotypic mice (in this case, WT and *Ifng1*$^{-/-}$ mice).

highly virulent in IFN-γ-deficient mice, respectively.[48] To examine whether the differential behaviors are detected in the *in vivo* CRISPR screen, we conducted an *in vivo* CRISPR screen in WT and *Ifngr1*$^{-/-}$ mice (Figures 3A–3G). The distribution of *in vivo* fitness scores in each *Ifngr1*$^{-/-}$ mouse showed high correlation (n = 7, r = 0.85 ± 0.03) (Figure 3A; Tables S1C and S1D). We next investigated similarities in *in vivo* fitness scores between individual mice by hierarchical clustering and principal component analysis (Figure 3B). Notably, WT and *Ifngr1*$^{-/-}$ mice were separately assigned to different clusters in both analyses (Figure 3B), suggesting independent behaviors of the knockout libraries in the two mouse backgrounds. We then generated the rank-ordered plots of *in vivo* fitness scores for WT and *Ifngr1*$^{-/-}$ mice (Figure 3C and Table S1E). Although ROP5 and ROP18 showed highly negative scores in WT mice, they did not in *Ifngr1*$^{-/-}$ mice (Figure 3C and Table S1E). In sharp contrast, ROP9, GRA17, PLP1, and SAG1 displayed highly negative scores in both WT and *Ifngr1*$^{-/-}$ mice, indicating that the differential behaviors of ROP5 and ROP18 can be specifically detected in the *in vivo* CRISPR screen. Next, we compared *in vivo* fitness scores between WT and *Ifngr1*$^{-/-}$ mice (Figure 3D). It was noteworthy that not only ROP5 and ROP18 but also GRA12 and GRA45, both of which are shown to be IFN-γ-dependent *in vivo* fitness genes,[17,28] were located far from the regression line (Figure 3D). Next, we selected the highly ranked *in vivo* fitness genes and compared the difference of *in vivo* fitness scores between WT and *Ifngr1*$^{-/-}$ mice (Figure 3E and Table S1E). We then found that ROP5, ROP18, GRA12, and GRA45 were majorly highlighted with high significance in the gRNA levels between WT and *Ifngr1*$^{-/-}$ mice (Figure 3E and Table S1E). These results demonstrated that our *in vivo* CRISPR screen using WT and *Ifngr1*$^{-/-}$ mice can efficiently extract the four major IFN-γ-dependent *in vivo* fitness genes among 376 genes targeted in the rhoptry/DG sublibrary. Furthermore, we found minor but novel IFN-γ-dependent *in vivo* fitness genes such as RON11, RON1, and

GRA23 with significant differences (Figure 3E and Table S1E). To further test the possibility, WT and *Ifngr1*$^{-/-}$ mice were locally infected with each mutant parasite strain in addition to ΔROP18 parasites, and the survival rates were monitored (Figure 3F). Although WT mice infected with ΔRON11, ΔRON1, ΔGRA23, or ΔROP18 parasites survived markedly longer than those infected with WT parasites, the survival time was reduced for *Ifngr1*$^{-/-}$ mice infected with ΔRON11, ΔRON1, ΔGRA23, or ΔROP18 parasites compared with WT mice, but not for the WT parasite (Figure 3F). Collectively, these results demonstrate that the *in vivo* CRISPR screens combined with host genetics highlights IFN-γ-dependent *in vivo* fitness genes (Figure 3G).

Identification of novel and known *in vivo* fitness genes related to *Toxoplasma* endomembrane system and nucleus

To identify the non-ROP/GRA *in vivo* fitness using our *in vivo* CRISPR screen system, we next generated a new sublibrary targeting the endomembrane system and nucleus-related genes (hereafter called the endomembrane-nucleus sublibrary) (Figure S3A; Tables S2A and S2B). We excluded genes with *in vitro* HFF fitness scores less than −1.5 to reduce the size of the sublibrary.[15]

Next, we conducted *in vivo* CRISPR screens in WT mice. The high reproducibility of both *in vitro* and *in vivo* screens was confirmed (Figures S3B–S3D; Tables S2C and S2D). To identify novel *in vivo* fitness genes, we compared *in vitro* and *in vivo* fitness scores (Figures 4A and 4B; Table S2A). Among the control genes, ROP18 and GRA23 possessed negative *in vivo* scores and ranked highly, indicating the feasibility of the *in vivo* CRISPR screen using the endomembrane-nucleus sublibrary. These analyses highlighted that EPT1 (TGGT1_257510), RAB4 (TGGT1_257340), HMGB (TGGT1_210408), ALG2 (TGGT1_227790), DGAT1 (TGGT1_232730), GST2 (TGGT1_306030), and TGGT1_203160 (hypothetical protein) were located far from the regression line and near ROP18 (Figure 4A and Table S2A) and had positive *in vitro* scores but extremely negative *in vivo* scores (Figure 4B and Table S2A). To examine whether these genes affect virulence, we generated individual knockout strains (Figure S3E). WT mice were locally infected with these mutant strains and monitored for their survival rates (Figure 4C). ΔEPT1, ΔRAB4, ΔHMGB, ΔALG2, ΔDGAT1, ΔGST2, and ΔTGGT1_203160 parasites lost or significantly reduced virulence (Figure 4C). Consistent with our screen result, a previous study reported that ΔGST2 parasites were less virulent than WT parasites in peritoneal infection.[49] Inconsistent with our result, ΔHMGB parasites were previously shown to be virulent in the peritoneal infection model.[50] The contribution of EPT1, RAB4, ALG2, DGAT1, and TGGT1_203160 to virulence had not been examined in previous studies.[51–54] Taken together, the expanded *in vivo* CRISPR screen yields known and novel endomembrane- or nucleus-related *in vivo* fitness genes.

GST2 and TGGT1_203160 are major IFN-γ-dependent *in vivo* fitness genes among the endomembrane organelles and nucleus-related genes

Next, we searched for IFN-γ-dependent *in vivo* fitness genes using WT and *Ifngr1*$^{-/-}$ mice (Figures S3F, 4D, and 4E; Tables S2C and S2D). Among the highly ranked *in vivo* fitness genes (Figure 4B), GST2 and TGGT1_203160 were highlighted as two remarkable IFN-γ-dependent genes (Figures 4D and 4E; Table S2A). We locally inoculated ΔGST2, ΔTGGT1_203160, and ΔEPT1 strains into WT and *Ifngr1*$^{-/-}$ mice and monitored their survival rates (Figure 4F). Although WT mice infected with ΔGST2 and ΔTGGT1_203160 parasites survived longer than those infected with WT parasites (Figure 4C), all of the infected *Ifngr1*$^{-/-}$ mice succumbed much earlier than WT mice (Figure 4F). In sharp contrast, ΔEPT1 parasites were still avirulent in *Ifngr1*$^{-/-}$ mice as well as in WT mice (Figure 4F). Thus, GST2 and TGGT1_203160 were identified as novel IFN-γ-dependent *in vivo* fitness genes.

Identification of known and novel *in vivo* fitness genes related to *Toxoplasma* metabolism

We further generated an additional sublibrary targeting metabolism-related genes encoding proteins localized at cytosol, apicoplast, and mitochondrion (hereafter called the metabolism sublibrary) (Figure S4A; Tables S3A and S3B).[35] The high reproducibility of both *in vitro* and *in vivo* screens was confirmed (Figures S4B and S4C; Tables S3C and S3D). Comparing *in vitro* and *in vivo* fitness scores highlighted that PDX1 (TGGT1_237140), EF-P (TGGT1_258380), TGGT1_204350 (hypothetical protein), PTS (TGGT1_305800), PDX2 (TGGT1_281490), and TGGT1_211695 (hypothetical protein) were located far from the regression line (Figures 5A and 5B; Table S3A). To examine whether these genes affect virulence, we generated individual knockout strains (Figure S4D) but failed to obtain ΔPTS parasites for unknown reasons. WT mice were locally infected with these mutant strains and monitored for their survival rates (Figure 5C). Although WT mice infected with ΔTGGT1_211695 parasites succumbed in a time course similar to that for WT parasites, all or most of mice infected with ΔPDX1, ΔEF-P, ΔTGGT1_204350, or ΔPDX2 parasites survived over the infection period (Figure 5C). PDX1 and PDX2 were shown to be required for *de novo* synthesis of vitamin B6 *in vivo*, and ΔPDX1 parasites lost virulence.[55] In accordance with this, PDX1 and PDX2 were ranked highly in our *in vivo* CRISPR screen (Figure 5B). In contrast, pyridoxal kinase (PLK), which is involved in salvage of vitamin B6, was ranked much lower (Figure 5B), consistent with the dispensable role of PLK in virulence.[55]

TGGT1_215890, USPase, Rad23, HID1, and Sui1 are novel IFN-γ-dependent metabolism-related *in vivo* fitness genes

To search for metabolism-related IFN-γ-dependent *in vivo* fitness genes, we next conducted an *in vivo* CRISPR screen in *Ifngr1*$^{-/-}$ mice (Figure S4E; Tables S3C and S3D). Comparing *in vivo* fitness scores between WT and *Ifngr1*$^{-/-}$ mice, TGGT1_215890 (hypothetical protein), USPase (TGGT1_218200), Rad23 (TGGT1_295340), HID1 (TGGT1_235490), and Sui1 (TGGT1_257060) were highlighted as IFN-γ-dependent *in vivo* fitness genes (Figures 5B, 5D, and 5E; Table S3A). We generated individual knockout strains (Figure S4D), which were inoculated to WT and *Ifngr1*$^{-/-}$ mice to compare the survival (Figure 5F). Although WT mice infected with ΔTGGT1_215890, ΔUSPase, ΔRad23, ΔHID1, and ΔSui1 parasites survived longer than those

CellPress
OPEN ACCESS

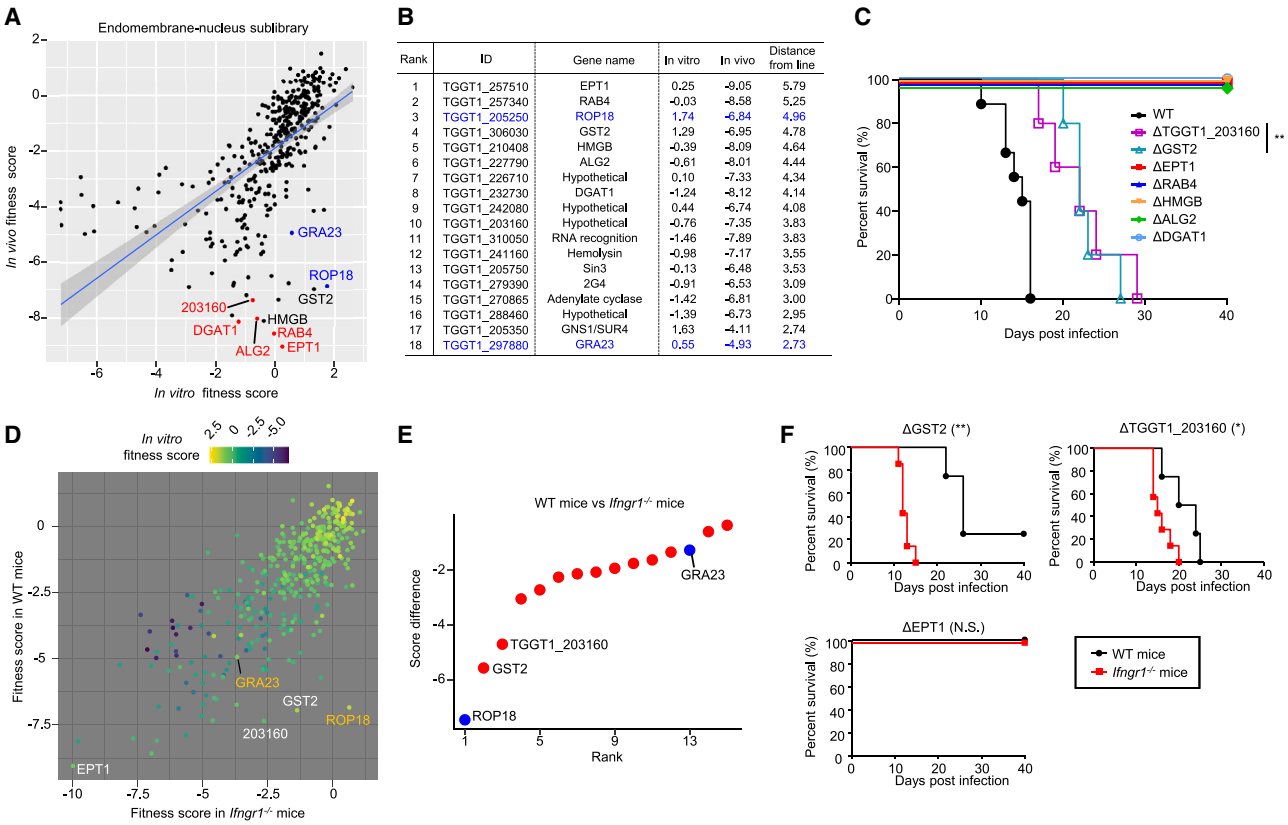

Rank	ID	Gene name	In vitro	In vivo	Distance from line
1	TGGT1_257510	EPT1	0.25	-9.05	5.79
2	TGGT1_257340	RAB4	-0.03	-8.58	5.25
3	TGGT1_205250	ROP18	1.74	-6.84	4.96
4	TGGT1_306030	GST2	1.29	-6.95	4.78
5	TGGT1_210408	HMGB	-0.39	-8.09	4.64
6	TGGT1_227790	ALG2	-0.61	-8.01	4.44
7	TGGT1_226710	Hypothetical	0.10	-7.33	4.34
8	TGGT1_232730	DGAT1	-1.24	-8.12	4.14
9	TGGT1_242080	Hypothetical	0.44	-6.74	4.08
10	TGGT1_203160	Hypothetical	-0.76	-7.35	3.83
11	TGGT1_310050	RNA recognition	-1.46	-7.89	3.83
12	TGGT1_241160	Hemolysin	-0.98	-7.17	3.55
13	TGGT1_205750	Sin3	-0.13	-6.48	3.53
14	TGGT1_279390	2G4	-0.91	-6.53	3.09
15	TGGT1_270865	Adenylate cyclase	-1.42	-6.81	3.00
16	TGGT1_288460	Hypothetical	-1.39	-6.73	2.95
17	TGGT1_205350	GNS1/SUR4	1.63	-4.11	2.74
18	TGGT1_297880	GRA23	0.55	-4.93	2.73

Figure 4. Identification of *Toxoplasma* endomembrane or nucleus-related virulence genes

(A) Scatterplot showing *in vitro* and *in vivo* fitness. Examples of previously reported and unreported virulence genes are labeled with black and red, respectively. ROP18 and GRA23 as control genes are labeled in blue.

(B) Ranking table for *in vivo* fitness genes ordered by the distance from the regression line. Lanes of ROP18 and GRA23 as virulence genes (internal control genes) are labeled in blue.

(C) Survival curves of WT mice with intra-footpad infection of 10^3 tachyzoites of the indicated knockout strains. Parasite genotype (mouse numbers tested): WT (n = 9), ΔEPT1 (n = 5), ΔRAB4 (n = 5), ΔHMGB (n = 5), ΔALG2 (n = 5), ΔDGAT1 (n = 5), ΔTGGT1_203160 (n = 5), and ΔGST2 (n = 5). **p < 0.01 (log-rank test).

(D) Scatterplot showing WT and *Ifngr1*$^{-/-}$ mice fitness scores. Example of IFN-γ-dependent *in vivo* fitness candidates are labeled in white. The color of each gene indicates the *in vitro* fitness score.

(E) The difference between WT and *Ifngr1*$^{-/-}$ mice fitness scores are calculated and ranked by the order. Plotted genes are selected with *in vitro* fitness score > −1.5, WT-*Ifngr1*$^{-/-}$ < 0, WT fitness score < −4, distance >2.7. Significant genes (p < 0.05, Wilcoxon rank-sum test) are marked in red.

(F) Survival curves of WT or *Ifngr1*$^{-/-}$ mice with intra-footpad infection of 10^3 tachyzoites of the indicated genes. Mouse genotype/parasite genotype (mouse numbers tested): WT/ΔTGGT1_203160 (n = 4), *Ifngr1*$^{-/-}$/ΔTGGT1_203160 (n = 7), WT/ΔGST2 (n = 4), *Ifngr1*$^{-/-}$/ΔGST2 (n = 7), WT/ΔEPT1 (n = 5), and *Ifngr1*$^{-/-}$/ΔEPT1 (n = 8). **p < 0.01; *p < 0.05; N.S., not significant (log-rank test).

See also Figure S3.

infected with WT parasites (Figures 5C and 5F), all of the infected *Ifngr1*$^{-/-}$ mice succumbed much earlier than WT mice (Figure 5F). On the other hand, ΔEF-P parasites were avirulent in both WT mice and *Ifngr1*$^{-/-}$mice (Figure 5F). Thus, TGGT1_215890, USPase, HID1, and Sui1 were identified as novel IFN-γ-dependent *in vivo* fitness genes.

GRA72 is required for correct localization of GRA17 and GRA23

Since GRA72 deletion resulted in significant loss of virulence (Figure 2E), we decided to focus on this novel GRA protein. GRA72 is a 57 kDa protein and possesses two transmembrane domains but lacks any other predicted functional domains (Figure S5A). GRA72 is well conserved between *Toxoplasma* strains (Figure S5B), and its orthologs are conserved within the subfamily of Toxoplasmatinae (Figure S5C). We noticed that most parasitophorous vacuoles (PVs) in mouse embryonic fibroblasts (MEFs) infected with ΔGRA72 parasites exhibited an enlarged "balloon-like" appearance (Figure 6A). Since this phenotype was quite reminiscent of the ΔGRA17 parasite (Figure 6A),[37] we considered a potential link between GRA72 and GRA17. To test this, we first analyzed GRA17 protein expression levels by western blot using anti-GRA17 antibody (Figures 6B, S5D, and S5E). GRA17 protein expression levels were comparable between WT and ΔGRA72 parasites (Figure 6B), suggesting that the phenotype of ΔGRA72 parasites was not due to aberrant GRA17 protein expression. Next, we analyzed the localization of GRA17 in ΔGRA72 parasites by immunofluorescence assay

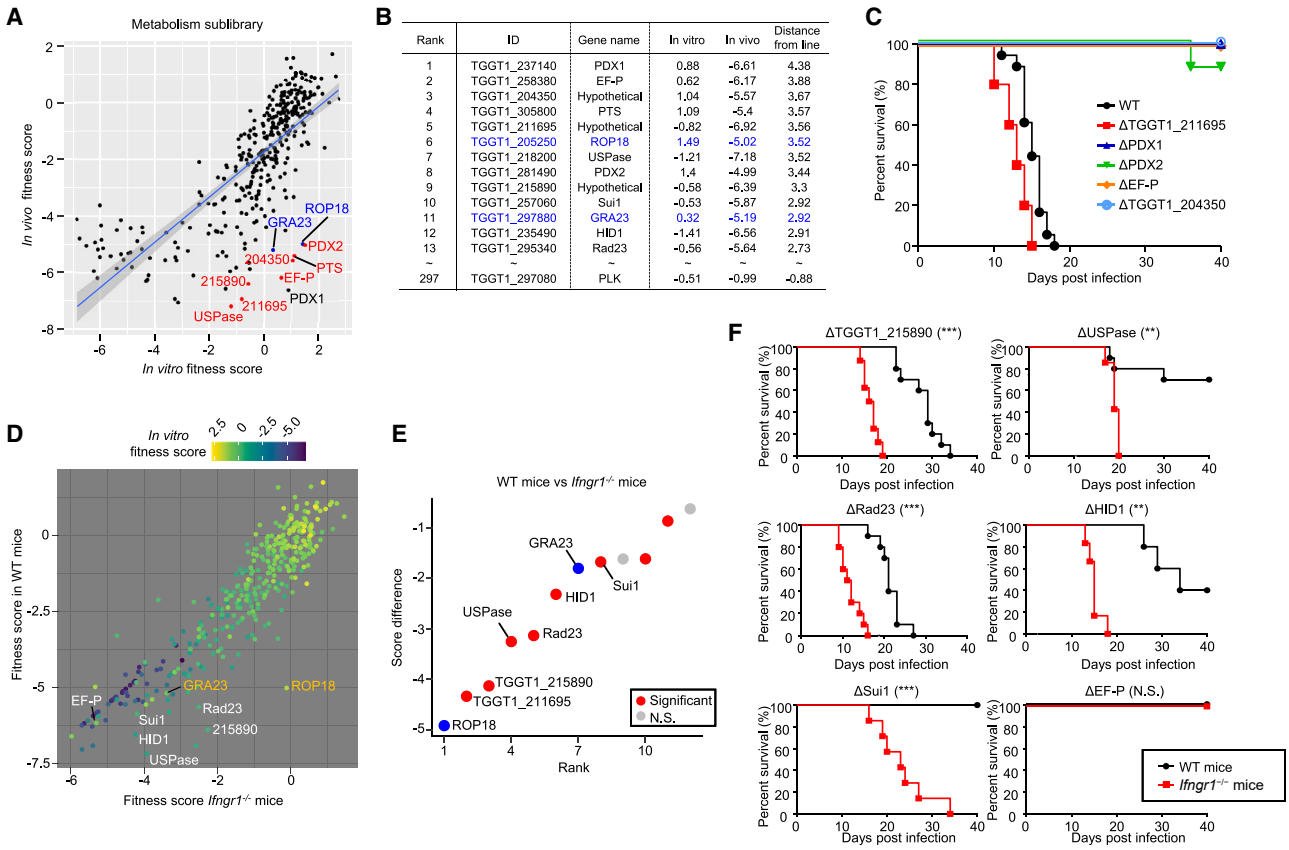

Rank	ID	Gene name	In vitro	In vivo	Distance from line
1	TGGT1_237140	PDX1	0.88	-6.61	4.38
2	TGGT1_258380	EF-P	0.62	-6.17	3.88
3	TGGT1_204350	Hypothetical	1.04	-5.57	3.67
4	TGGT1_305800	PTS	1.09	-5.4	3.57
5	TGGT1_211695	Hypothetical	-0.82	-6.92	3.56
6	TGGT1_205250	ROP18	1.49	-5.02	3.52
7	TGGT1_218200	USPase	-1.21	-7.18	3.52
8	TGGT1_281490	PDX2	1.4	-4.99	3.44
9	TGGT1_215890	Hypothetical	-0.58	-6.39	3.3
10	TGGT1_257060	Sui1	-0.53	-5.87	2.92
11	TGGT1_297880	GRA23	0.32	-5.19	2.92
12	TGGT1_235490	HID1	-1.41	-6.56	2.91
13	TGGT1_295340	Rad23	-0.56	-5.64	2.73
~	~	~	~	~	~
297	TGGT1_297080	PLK	-0.51	-0.99	-0.88

Figure 5. Identification of *Toxoplasma* metabolism-related virulence genes

(A) Scatterplot showing *in vitro* and *in vivo* fitness scores of each gene. Examples of previously reported and unreported virulence genes are labeled in black and red, respectively. ROP18 and GRA23 as control genes are labeled in blue.

(B) Ranking table for *in vivo* fitness genes ordered by the distance from the regression line. Lanes of ROP18 and GRA23 as internal control genes are labeled in blue.

(C) Survival curves of WT mice with intra-footpad infection of 10^3 tachyzoites of the indicated knockout strains. Parasite genotype (mouse numbers tested): WT (n = 18), ΔTGGT1_211695 (n = 5), ΔPDX1 (n = 8), ΔPDX2 (n = 9), ΔEF-P (n = 9), and ΔTGGT1_204350 (n = 5).

(D) Scatterplot showing WT and *Ifngr1*$^{-/-}$ mice fitness scores. Example of IFN-γ-dependent *in vivo* fitness candidates are labeled in white. The color of each gene indicates the *in vitro* fitness score.

(E) The difference between WT and *Ifngr1*$^{-/-}$ mice fitness scores are calculated and ranked by the order. Plotted genes are selected with *in vitro* fitness score > −1.5, WT-*Ifngr1*$^{-/-}$ < 0, WT fitness score < −4, distance > 2.7. Significant genes ($p < 0.05$, Wilcoxon rank-sum test) are marked in red. N.S., not significant.

(F) Survival curves of WT or *Ifngr1*$^{-/-}$ mice with intra-footpad infection of 10^3 tachyzoites of the indicated knockout strains. Mouse genotype/parasite genotype (mouse numbers tested): WT/ΔTGGT1_215890 (n = 10), *Ifngr1*$^{-/-}$/ΔTGGT1_215890 (n = 8), WT/ΔUSPase (n = 10), *Ifngr1*$^{-/-}$/ΔUSPase (n = 7), WT/ΔRad23 (n = 10), *Ifngr1*$^{-/-}$/ΔRad23 (n = 10), WT/ΔHID1 (n = 5), *Ifngr1*$^{-/-}$/ΔHID1 (n = 6), WT/ΔSui1 (n = 7), *Ifngr1*$^{-/-}$/ΔSui1 (n = 7), WT/ΔEF-P (n = 5), and *Ifngr1*$^{-/-}$/ΔEF-P (n = 5). ***$p < 0.001$; **$p < 0.01$; N.S., not significant (log-rank test).

See also Figure S4.

(IFA) (Figure 6C). As previously reported,[37] GRA17 was detected on parasitophorous vacuole membrane (PVM) in WT parasites (Figures 6C and S5E). In sharp contrast, GRA17 was highly aggregated and mislocalized in ΔGRA72 parasites (Figure 6C), indicating that the GRA17 mislocalization might account for aberrant PVs in ΔGRA72. To further characterize the relation between GRA72 and GRA17, we generated a complemented ΔGRA72 strain with C-terminal hemagglutinin (HA)-tagged GRA72 expressed from the SAG1 promoter, which we will refer to as "ΔGRA72 + GRA72-HA" (Figures 6B and S5F). The abnormality of PVs observed in ΔGRA72 parasites was completely rescued, and GRA17 localized on PVM in ΔGRA72 + GRA72-HA parasites (Figures 6A and 6C). In addition, the virulence of ΔGRA72 + GRA72-HA parasites was comparable with that of WT parasites (Figure 6D), indicating that the GRA72-HA is functional. We then analyzed the localization of GRA72-HA and GRA17 or GRA7 in the ΔGRA72 + GRA72-HA parasite-infected cells (Figures 6E and 6F). In contrast to GRA17 and GRA7, both of which localized on PVM uniformly, GRA72-HA protein localized unevenly (Figures 6E, 6F, S6G, and S6H). GRA23 is a paralog of GRA17 in *Toxoplasma*.[37] In addition, ΔGRA23 type II parasites showed the balloon-like PV phenotype like that of ΔGRA17 or ΔGRA72 type I parasites.[44] Therefore, we analyzed whether GRA72 is also involved in GRA23 localization. The HA

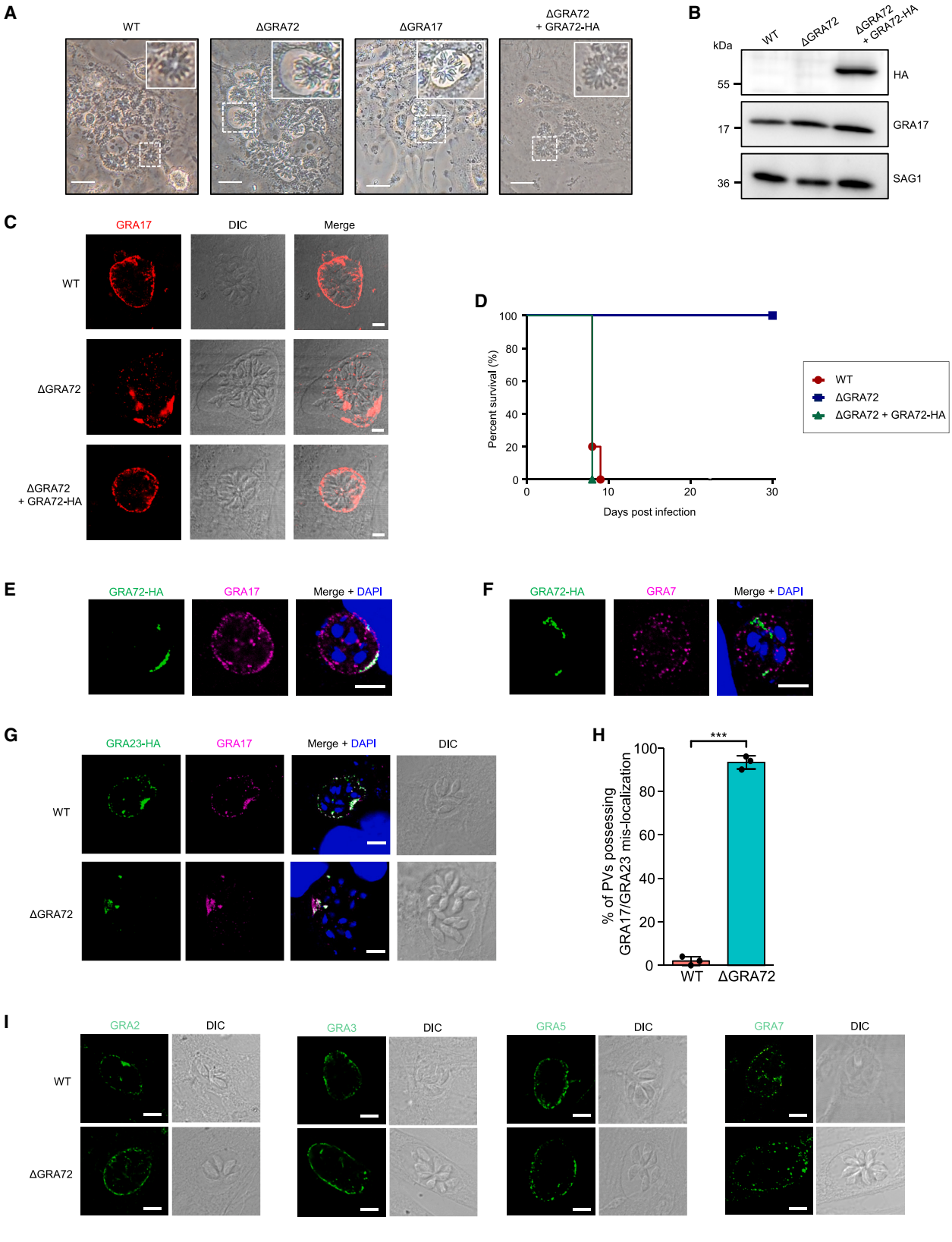

(legend on next page)

tag was endogenously inserted at the C terminus of GRA23 by genome editing in WT and ΔGRA72 parasites (Figures 6G and S6I). The HA-tagged GRA23 was colocalized with endogenous GRA17 in the transfected WT and ΔGRA72 parasites. The colocalization was uniformly detected on PVM in WT parasites but highly aggregated in ΔGRA72 parasites (Figures 6G and S6I), suggesting that GRA72 is involved in the correct localization of GRA23 as well as GRA17. Almost 90% of ΔGRA72 *Toxoplasma* PVs displayed GRA17/GRA23 mislocalization (Figure 6H). To investigate whether deletion of GRA72 affects not only GRA17 and GRA23 but also other PV-resident GRAs, we examined several PV-resident GRAs such as GRA2, GRA3, GRA5, and GRA7 (Figure 6I). We did not observe obvious differences of these GRA localizations between WT and ΔGRA72 parasites (Figure 6I). Altogether, these results demonstrated the biological links between GRA72 and GRA17/GRA23.

The UFMylation pathway contributes to *Toxoplasma* virulence

We searched for hidden biological interconnections across the three sublibraries and noticed that metabolism-related and endomembrane-nucleus-related *in vivo* fitness genes contained UFM1 (TGGT1_311110), UBA5 (TGGT1_231940), UFC1 (TGGT1_213830), UFL1 (TGGT1_222360), and UFSP (TGGT1_216020) (Figures 7A and 7B; Tables S2A and S3A). All of these are related to a fundamental biological process called UFMylation that is highly conserved in almost all eukaryotes except for fungi.[56,57] UFM1 is a ubiquitin-like protein and highly conserved in most apicomplexans except for *Plasmodium* spp. (Figures 7C and S6A).[58] Analogous to ubiquitination, the precursor UFM1 is processed by the specific peptidase (UFSP) in its C-terminal region, and a glycine residue needs to be exposed to become the mature UFM1.[59] UFM1 is then conjugated to target proteins by E1-like activating enzyme UBA5, E2-like conjugating enzyme UFC1,[57] and E3-like ligase UFL1, forming UFMylation.[60] To confirm whether UFM1 is involved in *in vivo* fitness, we generated ΔUFM1 parasites (Figure S6B). We locally infected WT mice with WT or ΔUFM1 parasites and monitored the survival (Figure 7D). WT mice infected with ΔUFM1 survived longer than those infected with WT parasites (Figure 7D). We found that the C-terminal glycine residue (G87) is conserved in TgUFM1 (Figure 7C). Therefore, we examined whether this glycine residue is important for UFM1-mediated *in vivo* fitness of *Toxoplasma*. ΔUFM1 parasites were complemented with the N-terminal FLAG-tagged WT (ΔUFM1 + UFM1 (WT)) or a mutant of UFM1 (ΔUFM1 + UFM1 (G87A)) (Figures 7E and S6C) and tested for the virulence in WT mice (Figure 7D). ΔUFM1 + UFM1 (WT) parasites restored virulence fully, whereas ΔUFM1 + UFM1 (G87A) parasites remained less virulent, similar to ΔUFM1 parasites (Figure 7D), indicating that the C-terminal glycine is required for UFM1-mediated *in vivo* fitness of *Toxoplasma*. Furthermore, it was of interest that the UFMylation-related genes are likely IFN-γ-dependent *in vivo* fitness genes, since we found that fitness scores of the UFMylation-related genes in *Ifngr1*$^{-/-}$ mice were significantly higher than those of WT mice (Figure 7B). In line with this observation, ΔUFM1 parasites restored virulence in *Ifngr1*$^{-/-}$ mice (Figure 7F). Taken together, the *in vivo* CRISPR screen highlighted *Toxoplasma* UFMylation-related genes in the IFN-γ-dependent *in vivo* fitness program.

DISCUSSION

Although there have been four *in vivo* CRISPR screens in microbiology so far,[16–18,61] this study is the first examination to classify virulence genes by a combination of host genetics and *in vivo* CRISPR screen. We clearly demonstrated that the *in vivo* fitness genes of *Toxoplasma* could be classified by the IFN-γ dependence by comparing the screen results between WT and *Ifngr1*$^{-/-}$ mice. Compared with ROP/GRA,[62] it was not known that RONs such as RON11 and RON1 play a role in IFN-γ-dependent *in vivo* fitness. We have developed this screen system using C57BL/6 mice. Given that many gene-manipulated mice are prepared in the C57BL/6 genetic background, the use of C57BL/6 mice in *Toxoplasma in vivo* CRISPR screens would ease interpretation of screen results and the subsequent immunological studies.

The lists in this study contain rankings of *in vivo* fitness genes, which are determined by the distance from the regression line. The top-ranking genes in each sublibrary were shown to affect virulence essentially (ROP5, PLP1, Clptm1, GRA17, and PDX1)[3,4,17,37,55,63,64] or modestly (ROP9, GRA12, and ROP18),[11,28,38,45] suggesting high correlation between the

Figure 6. GRA72 is required for correct localization of GRA17 and GRA23

(A) Representative images of PV morphology of WT, ΔGRA72, ΔGRA17, and ΔGRA72 + GRA72-HA parasites. MEFs were infected with the indicated parasites for 36 h and imaged by phase-contrast microscopy. Scale bars, 25 μm. Insets show one of the PVs in the indicated parasites.

(B) Assessment of GRA17 protein expression levels by western blotting in WT, ΔGRA72, and ΔGRA72 + GRA72-HA parasites.

(C) Representative images of GRA17 localization. MEFs were infected with the indicated parasites for 48 h, then fixed and subjected to IFA with anti-GRA17 antibody (red). Scale bars, 5 μm.

(D) Survival curves of mice intraperitoneally infected with 10^3 tachyzoites of WT (n = 5), ΔGRA72 (n = 5), or ΔGRA72 + GRA72-HA (n = 5).

(E and F) Localizations of GRA72-HA and GRA17 (E) or GRA7 (F) were assessed by IFA. MEFs were infected with ΔGRA72 + GRA72-HA parasites for 24 h and subjected to IFA with anti-HA (green) and anti-GRA17 (E) or anti-GRA7 (F) antibody (magenta). Representative images are shown. Scale bars, 5 μm.

(G) A C-terminal HA tagging of GRA23 in WT or ΔGRA72 parasites. The endogenous tagged parasites were subjected to IFA with anti-HA (green) and anti-GRA17 antibody (magenta). Representative images are shown. Scale bars, 5 μm.

(H) Localization of GRA17/GRA23 were observed and assessed as normal localization (uniformly on PVM) or mislocalization (see G and Figure S5I). A total of 50 PVs containing more than four parasites were observed. Data are displayed as mean values (n = 3). Error bars represent SD. ***p < 0.001 (Welch two-sample t test).

(I) Representative images of localizations of GRA2, GRA3, GRA5, or GRA7. MEFs were infected with WT or ΔGRA72 parasites for 24 h, then fixed and subjected to IFA with antibody against the indicated GRA (green). Scale bars, 5 μm.

DIC, differential interference contrast. See also Figure S5.

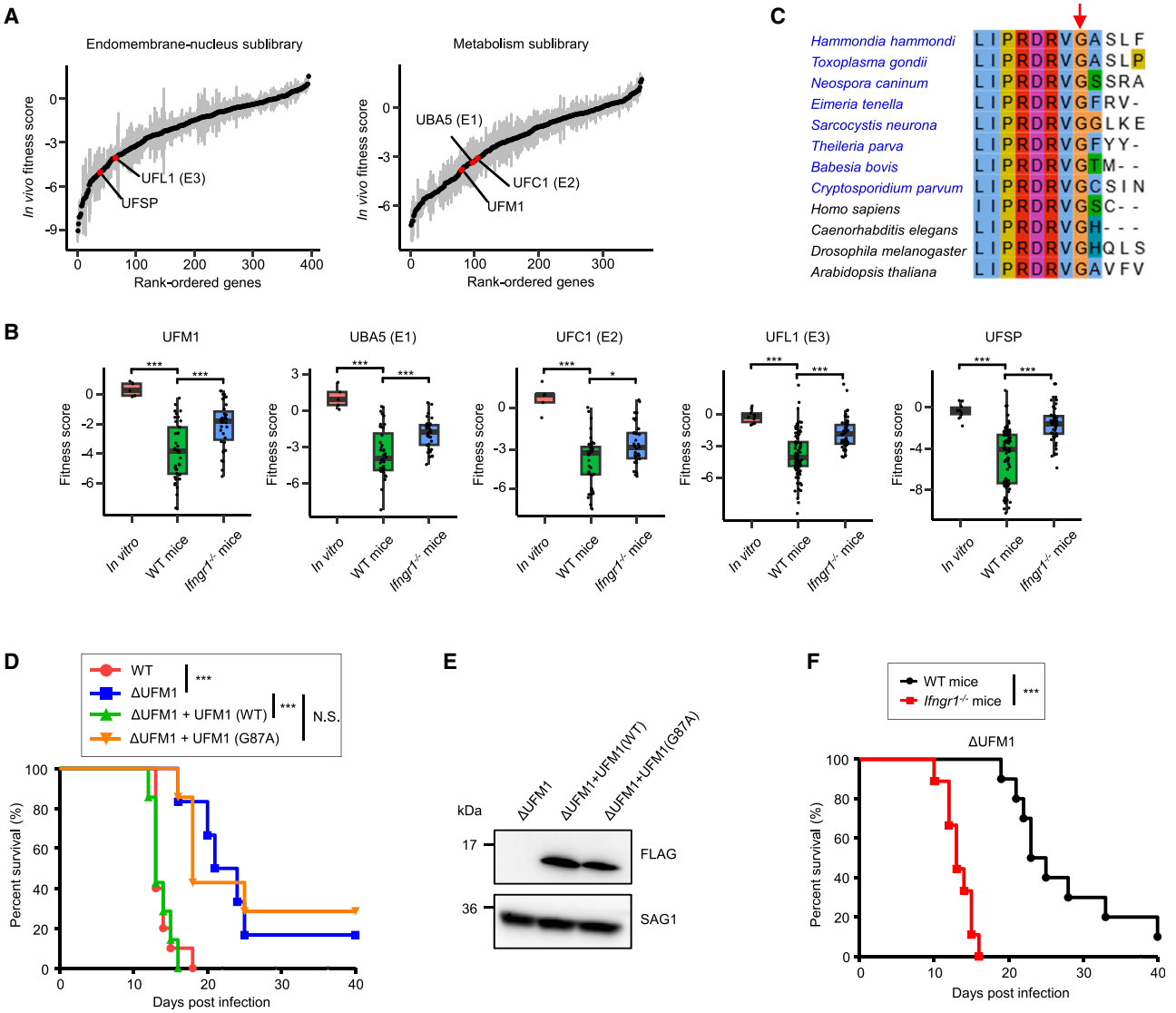

Figure 7. The UFMylation pathway contributes to *Toxoplasma* virulence

(A) Rank-ordered plots for *in vivo* fitness scores from the endomembrane-nucleus sublibrary (left) and the metabolism sublibrary (right). UFMylation-related genes are marked in red. Error bars (gray) represent SEM.

(B) Fitness scores of the UFMylation-related genes in Vero cells (*in vitro*), WT mice (WT), and *Ifngr1*$^{-/-}$ mice (KO) are shown as box plots. Each dot represents fitness scores for individual gRNAs. ***p < 0.001; *p < 0.05 (Wilcoxon rank-sum test).

(C) The conserved C-terminal amino acid sequences of the UFM1 homologs from indicated apicomplexan (blue) and model organisms (black). The conserved glycine residue is shown by the arrow.

(D) Survival curves of WT mice with intra-footpad infection of 10^3 tachyzoites of WT (n = 10), ΔUFM1 (n = 6), ΔUFM1 + UFM1 (WT) (n = 7), and ΔUFM1 + UFM1 (G87A) (n = 7). ***p < 0.001; N.S., not significant (log-rank test).

(E) Complementations of FLAG-tagged WT and G87A UFM1 protein in ΔUFM1 parasites.

(F) Survival curves of WT (n = 10) or *Ifngr1*$^{-/-}$ (n = 9) mice with intra-footpad infection of 10^3 tachyzoites of ΔUFM1 parasites. ***p < 0.001 (log-rank test).

See also Figure S6.

ranking and virulence. In contrast, despite being ranked highly in our screen results, GRA23, HMGB, and Rad23 were previously shown to be dispensable for virulence in the intraperitoneal infection model.[37,50,65] Given that GRA23, HMGB, and Rad23 affect virulence in the footpad infection, the intraperitoneal infection may negate *in vivo* fitness differences in the knockout parasites.[46,47] In contrast, TGGT1_211695 was ranked highly; however, ΔTGGT1_211695 parasites were still virulent. We speculate that this discrepancy might arise from the conditions between *in vivo* CRISPR screen and virulence validation, which are quite different (pooled with hundreds of other mutants or ΔTGGT1_211695 parasite alone, respectively).

In addition, although GRA6, GRA7 and ROP17 were previously shown to affect virulence,[26,27,46] they were not ranked highly in our screen. Given that the *in vivo* gRNA levels of GRA6, GRA7, and ROP17 were significantly less than the *in vitro* levels (Table S1A), they might be *in vivo* fitness genes albeit weakly. It is reported that phenotypes of ΔGRA7ΔROP18 or ΔROP17ΔROP18 double-knockout parasites are as severe as those of ΔROP5 parasites.[26,27] Therefore, if ΔROP18 parasites are used for the *in vivo* CRISPR screen, GRA7 and ROP17 could be ranked as highly as ROP5. It would be interesting to perform an *in vivo* CRISPR screen between WT and gene-knockout parasites to identify "synthetic lethal-like" pairs of *in vivo* fitness genes.

We show that GRA72 is involved in the correct localization of GRA17 and GRA23 on PVM but not for other GRAs tested in this study. It remains unclear whether GRA72 directly interacts with GRA17 and GRA23 or how GRA72 regulates their correct localization. In *Toxoplasma*, GRA17 and GRA23 comprise membrane pores that allow for the exchange of small molecules between parasite and host across the PVM.[37] On the other hand, GRA17 and GRA23 are orthologs of *Plasmodium* EXP2, an essential component of PTEX translocon that transports various malarial effector proteins.[66] Given that deletion of GRA72, GRA17, and GRA23 resulted in an abnormal PV appearance, GRA72 in combination with GRA17 and GRA23 might be involved in the export of small molecules (and possibly proteins) to maintain normal PVM. GRA23 was identified as a significant IFN-γ-dependent gene in our screen but GRA17 was not. In addition, GRA72 is weakly IFN-γ dependent, since the *in vivo* fitness scores in WT and *Ifngr1*$^{-/-}$ mice were significantly different before p-value correction (Table S1E). Given that GRA72 regulates the localization of both GRA17 and GRA23, the weak IFN-γ dependence of GRA72 might be explained by combined roles of the IFN-γ-dependent GRA23 and IFN-γ-independent GRA17, which is consistent with GRA23 and GRA72 being very recently identified as IFN-γ-dependent genes in human fibroblast via *in vitro* CRISPR screen.[67]

We demonstrate that UFMylation-related genes are highlighted as IFN-γ-dependent *in vivo* fitness genes. The introduction of G87A UFM1 mutant, defective in UFMylation into ΔUFM1 parasites, failed to restore the virulence, suggesting that UFMylation on target proteins might be important for parasite *in vivo* fitness. Identification of the UFMylated proteins is required to reveal the molecular mechanisms of the UFM1-dependent virulence program.

In conclusion, we have demonstrated that host genetics in combination with our newly developed *in vivo* CRISPR screen system yields various novel and known IFN-γ-dependent and independent *in vivo* fitness genes that affect virulence. Not only gene-knockout mice but also other mouse models such as humanized mice (e.g., hu-NSG mice) or even other host organisms such as primates and birds may be used for the screens to identify *in vivo* fitness genes specific to different host environments depending on species.[32,68–70] Thus, this host-genetics-empowered *in vivo* CRISPR screen system may help us to investigate *Toxoplasma* virulence genes against various host bottlenecks and find new aspects of this organism as well as therapeutics against toxoplasmosis.

Limitations of the study

The top hits of IFN-γ-dependent virulence factors such as ROP5, ROP18, GRA12, and GRA45 from our screen have been previously identified. Moreover, although we identified novel factors responsible for higher *Toxoplasma* infectivity in WT mice or *Ifngr1*$^{-/-}$ mice, additional efforts to address critical insights would be required. For instance, validations using cell-lineage-specific *Ifngr1* conditional knockout mice or mice lacking genes encoding IFN-γ-inducible effectors such as immunity-related GTPases, guanylate-binding proteins, inducible nitric oxide synthase, or indole-2,3-dioxygenase could further unravel roles of the IFN-γ-dependent virulence factors in the future.

STAR★METHODS

Detailed methods are provided in the online version of this paper and include the following:

- KEY RESOURCES TABLE
- RESOURCE AVAILABILITY
  - Lead contact
  - Materials availability
  - Data and code availability
- EXPERIMENTAL MODEL AND SUBJECT DETAILS
  - Toxoplasma strains
  - Host cell culture
  - Mice
- METHOD DETAILS
  - Plasmid construction for knockout *Toxoplasma*
  - Generation of gene knockout *Toxoplasma*
  - Complementation of GRA72 and UFM1
  - Generation of custom anti-GRA17 antibody
  - Immunofluorescence assay
  - Assessment of *in vivo* virulence in mice
  - Quantitative RT-PCR
  - Western blotting
  - Endogenous GRA23 tagging at the C terminus
  - *In vitro* and *in vivo* pooled CRISPR screens
  - Bioinformatic analysis of the CRISPR screen
  - GRA72 and UFM1 phylogenetic analysis
- QUANTIFICATION AND STATISTICAL ANALYSIS

SUPPLEMENTAL INFORMATION

Supplemental information can be found online at https://doi.org/10.1016/j.celrep.2023.112592.

ACKNOWLEDGMENTS

We thank M. Enomoto and N. Yamagishi (Osaka University) for secretarial and technical assistance. We thank Dr. J.C. Boothroyd for anti-GRA7 antibody. We thank Dr. D. Soldati-Favre for anti-GRA2 and GRA3 antibodies. This study was supported by Japan Science and Technology Agency (JPMJFR206D and JPMJMS2025); Agency for Medical Research and Development (JP20fk0108137, JP23fk0108682, and JP223fa627002); Ministry of Education, Culture, Sports, Science and Technology (20B304 and 19H00970); Japan Society for the Promotion of Science (23KJ1469); the program from Joint Usage and Joint Research Programs of the Institute of Advanced Medical Sciences, Tokushima University; Takeda Science Foundation; Mochida Memorial Foundation; Astellas Foundation for Research on

Metabolic Disorders; Naito Foundation; the Chemo-Sero-Therapeutic Research Institute; Research Foundation for Microbial Diseases of Osaka University; BIKEN Taniguchi Scholarship; The Nippon Foundation - Osaka University Project for Infectious Disease Prevention; and Joint Research Program of Research Center for Global and Local Infectious Diseases of Oita University (2021B06).

AUTHOR CONTRIBUTIONS

Conceptualization, Y.T. and M.Y.; methodology, Y.T. and M.Y.; software and formal analysis, Y.T.; investigation, Y.T., E.H., and M.Y.; writing – original draft, Y.T. and M.Y.; writing – review & editing, Y.T., M.S., and M.Y.; funding acquisition, M.Y.; supervision, M.Y.

DECLARATION OF INTERESTS

The authors declare no competing interests.

Received: February 6, 2023
Revised: April 25, 2023
Accepted: May 17, 2023
Published: June 1, 2023

REFERENCES

1. Montoya, J.G., and Remington, J.S. (2008). Management of Toxoplasma gondii infection during pregnancy. Clin. Infect. Dis. *47*, 554–566. https://doi.org/10.1086/590149.
2. Boothroyd, J.C. (2009). Toxoplasma gondii: 25 years and 25 major advances for the field. Int. J. Parasitol. *39*, 935–946. https://doi.org/10.1016/j.ijpara.2009.02.003.
3. Behnke, M.S., Khan, A., Wootton, J.C., Dubey, J.P., Tang, K., and Sibley, L.D. (2011). Virulence differences in Toxoplasma mediated by amplification of a family of polymorphic pseudokinases. Proc. Natl. Acad. Sci. USA *108*, 9631–9636. https://doi.org/10.1073/pnas.1015338108.
4. Reese, M.L., Zeiner, G.M., Saeij, J.P.J., Boothroyd, J.C., and Boyle, J.P. (2011). Polymorphic family of injected pseudokinases is paramount in Toxoplasma virulence. Proc. Natl. Acad. Sci. USA *108*, 9625–9630. https://doi.org/10.1073/pnas.1015980108.
5. Saeij, J.P.J., Boyle, J.P., Coller, S., Taylor, S., Sibley, L.D., Brooke-Powell, E.T., Ajioka, J.W., and Boothroyd, J.C. (2006). Polymorphic secreted kinases are key virulence factors in toxoplasmosis. Science *314*, 1780–1783. https://doi.org/10.1126/science.1133690.
6. Taylor, S., Barragan, A., Su, C., Fux, B., Fentress, S.J., Tang, K., Beatty, W.L., Hajj, H.E., Jerome, M., Behnke, M.S., et al. (2006). A secreted serine-threonine kinase determines virulence in the eukaryotic pathogen Toxoplasma gondii. Science *314*, 1776–1780. https://doi.org/10.1126/science.1133643.
7. Hunter, C.A., and Sibley, L.D. (2012). Modulation of innate immunity by Toxoplasma gondii virulence effectors. Nat. Rev. Microbiol. *10*, 766–778. https://doi.org/10.1038/nrmicro2858.
8. Sasai, M., and Yamamoto, M. (2022). Anti-Toxoplasma host defense systems and the parasitic counterdefense mechanisms. Parasitol. Int. *89*, 102593. https://doi.org/10.1016/j.parint.2022.102593.
9. Steinfeldt, T., Könen-Waisman, S., Tong, L., Pawlowski, N., Lamkemeyer, T., Sibley, L.D., Hunn, J.P., and Howard, J.C. (2010). Phosphorylation of mouse immunity-related GTPase (IRG) resistance proteins is an evasion strategy for virulent Toxoplasma gondii. PLoS Biol. *8*, e1000576. https://doi.org/10.1371/journal.pbio.1000576.
10. El Hajj, H., Lebrun, M., Fourmaux, M.N., Vial, H., and Dubremetz, J.F. (2007). Inverted topology of the Toxoplasma gondii ROP5 rhoptry protein provides new insights into the association of the ROP2 protein family with the parasitophorous vacuole membrane. Cell Microbiol. *9*, 54–64. https://doi.org/10.1111/j.1462-5822.2006.00767.x.
11. Fentress, S.J., Behnke, M.S., Dunay, I.R., Mashayekhi, M., Rommereim, L.M., Fox, B.A., Bzik, D.J., Taylor, G.A., Turk, B.E., Lichti, C.F., et al. (2010). Phosphorylation of immunity-related GTPases by a Toxoplasma gondii-secreted kinase promotes macrophage survival and virulence. Cell Host Microbe *8*, 484–495. https://doi.org/10.1016/j.chom.2010.11.005.
12. Selleck, E.M., Fentress, S.J., Beatty, W.L., Degrandi, D., Pfeffer, K., Virgin, H.W., 4th, Macmicking, J.D., and Sibley, L.D. (2013). Guanylate-binding protein 1 (Gbp1) contributes to cell-autonomous immunity against Toxoplasma gondii. PLoS Pathog. *9*, e1003320. https://doi.org/10.1371/journal.ppat.1003320.
13. Saeij, J.P.J., Coller, S., Boyle, J.P., Jerome, M.E., White, M.W., and Boothroyd, J.C. (2007). Toxoplasma co-opts host gene expression by injection of a polymorphic kinase homologue. Nature *445*, 324–327. https://doi.org/10.1038/nature05395.
14. Yamamoto, M., Standley, D.M., Takashima, S., Saiga, H., Okuyama, M., Kayama, H., Kubo, E., Ito, H., Takaura, M., Matsuda, T., et al. (2009). A single polymorphic amino acid on Toxoplasma gondii kinase ROP16 determines the direct and strain-specific activation of Stat3. J. Exp. Med. *206*, 2747–2760. https://doi.org/10.1084/jem.20091703.
15. Sidik, S.M., Huet, D., Ganesan, S.M., Huynh, M.H., Wang, T., Nasamu, A.S., Thiru, P., Saeij, J.P.J., Carruthers, V.B., Niles, J.C., and Lourido, S. (2016). A genome-wide CRISPR screen in Toxoplasma identifies essential apicomplexan genes. Cell *166*, 1423–1435.e12. https://doi.org/10.1016/j.cell.2016.08.019.
16. Sangare, L.O., Olafsson, E.B., Wang, Y., Yang, N., Julien, L., Camejo, A., Pesavento, P., Sidik, S.M., Lourido, S., Barragan, A., and Saeij, J.P.J. (2019). In vivo CRISPR screen identifies TgWIP as a Toxoplasma modulator of dendritic cell migration. Cell Host Microbe *26*, 478–492. https://doi.org/10.1016/j.chom.2019.09.008.
17. Young, J., Dominicus, C., Wagener, J., Butterworth, S., Ye, X., Kelly, G., Ordan, M., Saunders, B., Instrell, R., Howell, M., et al. (2019). A CRISPR platform for targeted in vivo screens identifies Toxoplasma gondii virulence factors in mice. Nat. Commun. *10*, 3963. https://doi.org/10.1038/s41467-019-11855-w.
18. Butterworth, S., Torelli, F., Lockyer, E.J., Wagener, J., Song, O.R., Broncel, M., Russell, M.R.G., Moreira-Souza, A.C.A., Young, J.C., and Treeck, M. (2022). Toxoplasma gondii virulence factor ROP1 reduces parasite susceptibility to murine and human innate immune restriction. PLoS Pathog. *18*, e1011021. https://doi.org/10.1371/journal.ppat.1011021.
19. Abel, S., Abel zur Wiesch, P., Davis, B.M., and Waldor, M.K. (2015). Analysis of bottlenecks in experimental models of infection. PLoS Pathog. *11*, e1004823. https://doi.org/10.1371/journal.ppat.1004823.
20. Frickel, E.M., and Hunter, C.A. (2021). Lessons from Toxoplasma: host responses that mediate parasite control and the microbial effectors that subvert them. J. Exp. Med. *218*, e20201314. https://doi.org/10.1084/jem.20201314.
21. Yarovinsky, F. (2014). Innate immunity to Toxoplasma gondii infection. Nat. Rev. Immunol. *14*, 109–121. https://doi.org/10.1038/nri3598.
22. Saeij, J.P., and Frickel, E.M. (2017). Exposing Toxoplasma gondii hiding inside the vacuole: a role for GBPs, autophagy and host cell death. Curr. Opin. Microbiol. *40*, 72–80. https://doi.org/10.1016/j.mib.2017.10.021.
23. Sasai, M., Pradipta, A., and Yamamoto, M. (2018). Host immune responses to Toxoplasma gondii. Int. Immunol. *30*, 113–119. https://doi.org/10.1093/intimm/dxy004.
24. Scharton-Kersten, T.M., Wynn, T.A., Denkers, E.Y., Bala, S., Grunvald, E., Hieny, S., Gazzinelli, R.T., and Sher, A. (1996). In the absence of endogenous IFN-gamma, mice develop unimpaired IL-12 responses to Toxoplasma gondii while failing to control acute infection. J. Immunol. *157*, 4045–4054.
25. Suzuki, Y., Orellana, M.A., Schreiber, R.D., and Remington, J.S. (1988). Interferon-gamma: the major mediator of resistance against Toxoplasma gondii. Science *240*, 516–518. https://doi.org/10.1126/science.3128869.

26. Etheridge, R.D., Alaganan, A., Tang, K., Lou, H.J., Turk, B.E., and Sibley, L.D. (2014). The Toxoplasma pseudokinase ROP5 forms complexes with ROP18 and ROP17 kinases that synergize to control acute virulence in mice. Cell Host Microbe *15*, 537–550. https://doi.org/10.1016/j.chom.2014.04.002.

27. Alaganan, A., Fentress, S.J., Tang, K., Wang, Q., and Sibley, L.D. (2014). Toxoplasma GRA7 effector increases turnover of immunity-related GTPases and contributes to acute virulence in the mouse. Proc. Natl. Acad. Sci. USA *111*, 1126–1131. https://doi.org/10.1073/pnas.1313501111.

28. Fox, B.A., Guevara, R.B., Rommereim, L.M., Falla, A., Bellini, V., Pètre, G., Rak, C., Cantillana, V., Dubremetz, J.F., Cesbron-Delauw, M.F., et al. (2019). Toxoplasma gondii parasitophorous vacuole membrane-associated dense granule proteins orchestrate chronic infection and GRA12 underpins resistance to host gamma interferon. mBio *10*, 005899-e619. https://doi.org/10.1128/mBio.00589-19.

29. Wang, Y., Sangaré, L.O., Paredes-Santos, T.C., Hassan, M.A., Krishnamurthy, S., Furuta, A.M., Markus, B.M., Lourido, S., and Saeij, J.P.J. (2020). Genome-wide screens identify Toxoplasma gondii determinants of parasite fitness in IFNgamma-activated murine macrophages. Nat. Commun. *11*, 5258. https://doi.org/10.1038/s41467-020-18991-8.

30. Seizova, S., Ruparel, U., Garnham, A.L., Bader, S.M., Uboldi, A.D., Coffey, M.J., Whitehead, L.W., Rogers, K.L., and Tonkin, C.J. (2022). Transcriptional modification of host cells harboring Toxoplasma gondii bradyzoites prevents IFN gamma-mediated cell death. Cell Host Microbe *30*, 232–247.e6. https://doi.org/10.1016/j.chom.2021.11.012.

31. Franco, M., Panas, M.W., Marino, N.D., Lee, M.C.W., Buchholz, K.R., Kelly, F.D., Bednarski, J.J., Sleckman, B.P., Pourmand, N., and Boothroyd, J.C. (2016). A novel secreted protein, MYR1, is central to toxoplasma's manipulation of host cells. mBio *7*, e02231-e02215. https://doi.org/10.1128/mBio.02231-15.

32. Bando, H., Sakaguchi, N., Lee, Y., Pradipta, A., Ma, J.S., Tanaka, S., Lai, D.H., Liu, J., Lun, Z.R., Nishikawa, Y., et al. (2018). Toxoplasma effector TgIST targets host Ido1 to antagonize the IFN-gamma-Induced anti-parasitic response in human cells. Front. Immunol. *9*, 2073. https://doi.org/10.3389/fimmu.2018.02073.

33. Gay, G., Braun, L., Brenier-Pinchart, M.P., Vollaire, J., Josserand, V., Bertini, R.L., Varesano, A., Touquet, B., De Bock, P.J., Coute, Y., et al. (2016). Toxoplasma gondii TgIST co-opts host chromatin repressors dampening STAT1-dependent gene regulation and IFN-gamma-mediated host defenses. J. Exp. Med. *213*, 1779–1798. https://doi.org/10.1084/jem.20160340.

34. Olias, P., Etheridge, R.D., Zhang, Y., Holtzman, M.J., and Sibley, L.D. (2016). Toxoplasma effector recruits the mi-2/NuRD complex to repress STAT1 transcription and block IFN-gamma-Dependent gene expression. Cell Host Microbe *20*, 72–82. https://doi.org/10.1016/j.chom.2016.06.006.

35. Barylyuk, K., Koreny, L., Ke, H., Butterworth, S., Crook, O.M., Lassadi, I., Gupta, V., Tromer, E., Mourier, T., Stevens, T.J., et al. (2020). A comprehensive subcellular atlas of the Toxoplasma proteome via hyperLOPIT provides spatial context for protein functions. Cell Host Microbe *28*, 752–766.e9. https://doi.org/10.1016/j.chom.2020.09.011.

36. Sidik, S.M., Huet, D., and Lourido, S. (2018). CRISPR-Cas9-based genome-wide screening of Toxoplasma gondii. Nat. Protoc. *13*, 307–323. https://doi.org/10.1038/nprot.2017.131.

37. Gold, D.A., Kaplan, A.D., Lis, A., Bett, G.C.L., Rosowski, E.E., Cirelli, K.M., Bougdour, A., Sidik, S.M., Beck, J.R., Lourido, S., et al. (2015). The Toxoplasma dense granule proteins GRA17 and GRA23 mediate the movement of small molecules between the host and the parasitophorous vacuole. Cell Host Microbe *17*, 642–652. https://doi.org/10.1016/j.chom.2015.04.003.

38. Dongchao, Z., Ning, J., and Qijun, C. (2020). Loss of rhoptry protein 9 impeded Toxoplasma gondii infectivity. Acta Trop. *207*, 105464. https://doi.org/10.1016/j.actatropica.2020.105464.

39. Bradley, P.J., Ward, C., Cheng, S.J., Alexander, D.L., Coller, S., Coombs, G.H., Dunn, J.D., Ferguson, D.J., Sanderson, S.J., Wastling, J.M., and Boothroyd, J.C. (2005). Proteomic analysis of rhoptry organelles reveals many novel constituents for host-parasite interactions in Toxoplasma gondii. J. Biol. Chem. *280*, 34245–34258. https://doi.org/10.1074/jbc.M504158200.

40. Butler, C.L., Lucas, O., Wuchty, S., Xue, B., Uversky, V.N., and White, M. (2014). Identifying novel cell cycle proteins in Apicomplexa parasites through co-expression decision analysis. PLoS One *9*, e97625. https://doi.org/10.1371/journal.pone.0097625.

41. Wang, K., Peng, E.D., Huang, A.S., Xia, D., Vermont, S.J., Lentini, G., Lebrun, M., Wastling, J.M., and Bradley, P.J. (2016). Identification of novel O-linked glycosylated Toxoplasma proteins by vicia villosa lectin chromatography. PLoS One *11*, e0150561. https://doi.org/10.1371/journal.pone.0150561.

42. Tu, V., Mayoral, J., Sugi, T., Tomita, T., Han, B., Ma, Y.F., and Weiss, L.M. (2019). Enrichment and proteomic characterization of the cyst wall from in vitro Toxoplasma gondii cysts. mBio *10*, 004699-e519. https://doi.org/10.1128/mBio.00469-19.

43. Tu, V., Tomita, T., Sugi, T., Mayoral, J., Han, B., Yakubu, R.R., Williams, T., Horta, A., Ma, Y., and Weiss, L.M. (2020). The Toxoplasma gondii cyst wall interactome. mBio *11*. https://doi.org/10.1128/mBio.02699-19.

44. Li, T.T., Wang, J.L., Liang, Q.L., Sun, L.X., Zhang, H.S., Zhang, Z.W., Zhu, X.Q., and Elsheikha, H.M. (2020). Effect of deletion of gra17 and gra23 genes on the growth, virulence, and immunogenicity of type II Toxoplasma gondii. Parasitol. Res. *119*, 2907–2916. https://doi.org/10.1007/s00436-020-06815-z.

45. Yamamoto, M., Ma, J.S., Mueller, C., Kamiyama, N., Saiga, H., Kubo, E., Kimura, T., Okamoto, T., Okuyama, M., Kayama, H., et al. (2011). ATF6-beta is a host cellular target of the Toxoplasma gondii virulence factor ROP18. J. Exp. Med. *208*, 1533–1546. https://doi.org/10.1084/jem.20101660.

46. Ma, J.S., Sasai, M., Ohshima, J., Lee, Y., Bando, H., Takeda, K., and Yamamoto, M. (2014). Selective and strain-specific NFAT4 activation by the Toxoplasma gondii polymorphic dense granule protein GRA6. J. Exp. Med. *211*, 2013–2032. https://doi.org/10.1084/jem.20131272.

47. Drewry, L.L., Jones, N.G., Wang, Q., Onken, M.D., Miller, M.J., and Sibley, L.D. (2019). The secreted kinase ROP17 promotes Toxoplasma gondii dissemination by hijacking monocyte tissue migration. Nat. Microbiol. *4*, 1951–1963. https://doi.org/10.1038/s41564-019-0504-8.

48. Behnke, M.S., Fentress, S.J., Mashayekhi, M., Li, L.X., Taylor, G.A., and Sibley, L.D. (2012). The polymorphic pseudokinase ROP5 controls virulence in Toxoplasma gondii by regulating the active kinase ROP18. PLoS Pathog. *8*, e1002992. https://doi.org/10.1371/journal.ppat.1002992.

49. Li, S., Liu, J., Zhang, H., Sun, Z., Ying, Z., Wu, Y., Xu, J., and Liu, Q. (2021). Toxoplasma gondii glutathione S-transferase 2 plays an important role in partial secretory protein transport. Faseb. J. *35*, e21352. https://doi.org/10.1096/fj.202001987RR.

50. Wang, H., Lei, T., Liu, J., Li, M., Nan, H., and Liu, Q. (2014). A nuclear factor of high mobility group box protein in Toxoplasma gondii. PLoS One *9*, e111993. https://doi.org/10.1371/journal.pone.0111993.

51. Quittnat, F., Nishikawa, Y., Stedman, T.T., Voelker, D.R., Choi, J.Y., Zahn, M.M., Murphy, R.C., Barkley, R.M., Pypaert, M., Joiner, K.A., and Coppens, I. (2004). On the biogenesis of lipid bodies in ancient eukaryotes: synthesis of triacylglycerols by a Toxoplasma DGAT1-related enzyme. Mol. Biochem. Parasitol. *138*, 107–122. https://doi.org/10.1016/j.molbiopara.2004.08.004.

52. Hartmann, A., Hellmund, M., Lucius, R., Voelker, D.R., and Gupta, N. (2014). Phosphatidylethanolamine synthesis in the parasite mitochondrion is required for efficient growth but dispensable for survival of Toxoplasma gondii. J. Biol. Chem. *289*, 6809–6824. https://doi.org/10.1074/jbc.M113.509406.

53. Kremer, K., Kamin, D., Rittweger, E., Wilkes, J., Flammer, H., Mahler, S., Heng, J., Tonkin, C.J., Langsley, G., Hell, S.W., et al. (2013). An

overexpression screen of Toxoplasma gondii Rab-GTPases reveals distinct transport routes to the micronemes. PLoS Pathog. *9*, e1003213. https://doi.org/10.1371/journal.ppat.1003213.

54. Gas-Pascual, E., Ichikawa, H.T., Sheikh, M.O., Serji, M.I., Deng, B., Mandalasi, M., Bandini, G., Samuelson, J., Wells, L., and West, C.M. (2019). CRISPR/Cas9 and glycomics tools for Toxoplasma glycobiology. J. Biol. Chem. *294*, 1104–1125. https://doi.org/10.1074/jbc.RA118.006072.

55. Krishnan, A., Kloehn, J., Lunghi, M., Chiappino-Pepe, A., Waldman, B.S., Nicolas, D., Varesio, E., Hehl, A., Lourido, S., Hatzimanikatis, V., and Soldati-Favre, D. (2020). Functional and computational genomics reveal unprecedented flexibility in stage-specific Toxoplasma metabolism. Cell Host Microbe *27*, 290–306.e11. https://doi.org/10.1016/j.chom.2020.01.002.

56. Cappadocia, L., and Lima, C.D. (2018). Ubiquitin-like protein conjugation: structures, chemistry, and mechanism. Chem. Rev. *118*, 889–918. https://doi.org/10.1021/acs.chemrev.6b00737.

57. Komatsu, M., Chiba, T., Tatsumi, K., Iemura, S.i., Tanida, I., Okazaki, N., Ueno, T., Kominami, E., Natsume, T., and Tanaka, K. (2004). A novel protein-conjugating system for Ufm1, a ubiquitin-fold modifier. EMBO J. *23*, 1977–1986. https://doi.org/10.1038/sj.emboj.7600205.

58. Karpiyevich, M., and Artavanis-Tsakonas, K. (2020). Ubiquitin-like modifiers: emerging regulators of Protozoan parasites. Biomolecules *10*. https://doi.org/10.3390/biom10101403.

59. Kang, S.H., Kim, G.R., Seong, M., Baek, S.H., Seol, J.H., Bang, O.S., Ovaa, H., Tatsumi, K., Komatsu, M., Tanaka, K., and Chung, C.H. (2007). Two novel ubiquitin-fold modifier 1 (Ufm1)-specific proteases, UfSP1 and UfSP2. J. Biol. Chem. *282*, 5256–5262. https://doi.org/10.1074/jbc.M610590200.

60. Yoo, H.M., Kang, S.H., Kim, J.Y., Lee, J.E., Seong, M.W., Lee, S.W., Ka, S.H., Sou, Y.S., Komatsu, M., Tanaka, K., et al. (2014). Modification of ASC1 by UFM1 is crucial for ERalpha transactivation and breast cancer development. Mol. Cell *56*, 261–274. https://doi.org/10.1016/j.molcel.2014.08.007.

61. Liu, X., Kimmey, J.M., Matarazzo, L., de Bakker, V., Van Maele, L., Sirard, J.C., Nizet, V., and Veening, J.W. (2021). Exploration of bacterial bottlenecks and Streptococcus pneumoniae pathogenesis by CRISPRi-seq. Cell Host Microbe *29*, 107–120.e6. https://doi.org/10.1016/j.chom.2020.10.001.

62. Hakimi, M.A., Olias, P., and Sibley, L.D. (2017). Toxoplasma effectors targeting host signaling and transcription. Clin. Microbiol. Rev. *30*, 615–645. https://doi.org/10.1128/CMR.00005-17.

63. Kafsack, B.F.C., Pena, J.D.O., Coppens, I., Ravindran, S., Boothroyd, J.C., and Carruthers, V.B. (2009). Rapid membrane disruption by a perforin-like protein facilitates parasite exit from host cells. Science *323*, 530–533. https://doi.org/10.1126/science.1165740.

64. Rachinel, N., Buzoni-Gatel, D., Dutta, C., Mennechet, F.J.D., Luangsay, S., Minns, L.A., Grigg, M.E., Tomavo, S., Boothroyd, J.C., and Kasper, L.H. (2004). The induction of acute ileitis by a single microbial antigen of Toxoplasma gondii. J. Immunol. *173*, 2725–2735. https://doi.org/10.4049/jimmunol.173.4.2725.

65. Zhang, H., Liu, J., Ying, Z., Li, S., Wu, Y., and Liu, Q. (2020). Toxoplasma gondii UBL-UBA shuttle proteins contribute to the degradation of ubiquitinylated proteins and are important for synchronous cell division and virulence. Faseb. J. *34*, 13711–13725. https://doi.org/10.1096/fj.202000759RR.

66. Beck, J.R., and Ho, C.M. (2021). Transport mechanisms at the malaria parasite-host cell interface. PLoS Pathog. *17*, e1009394. https://doi.org/10.1371/journal.ppat.1009394.

67. Krishnamurthy, S., Maru, P., Wang, Y., Bitew, M.A., Mukhopadhyay, D., Yamaryo-Botte, Y., Paredes-Santos, T.C., Sangare, L.O., Swale, C., Botte, C.Y., and Saeij, J.P.J. (2023). CRISPR screens identify Toxoplasma genes that determine parasite fitness in interferon gamma-stimulated human cells. mBio, e0006023. https://doi.org/10.1128/mbio.00060-23.

68. Sher, A., Tosh, K., and Jankovic, D. (2017). Innate recognition of Toxoplasma gondii in humans involves a mechanism distinct from that utilized by rodents. Cell. Mol. Immunol. *14*, 36–42. https://doi.org/10.1038/cmi.2016.12.

69. Gazzinelli, R.T., Mendonça-Neto, R., Lilue, J., Howard, J., and Sher, A. (2014). Innate resistance against Toxoplasma gondii: an evolutionary tale of mice, cats, and men. Cell Host Microbe *15*, 132–138. https://doi.org/10.1016/j.chom.2014.01.004.

70. Bando, H., Lee, Y., Sakaguchi, N., Pradipta, A., Ma, J.S., Tanaka, S., Cai, Y., Liu, J., Shen, J., Nishikawa, Y., et al. (2018). Inducible nitric oxide synthase is a key host factor for Toxoplasma GRA15-dependent disruption of the gamma interferon-induced antiparasitic human response. mBio *9*, 017388-e1818. https://doi.org/10.1128/mBio.01738-18.

71. Sasai, M., Sakaguchi, N., Ma, J.S., Nakamura, S., Kawabata, T., Bando, H., Lee, Y., Saitoh, T., Akira, S., Iwasaki, A., et al. (2017). Essential role for GABARAP autophagy proteins in interferon-inducible GTPase-mediated host defense. Nat. Immunol. *18*, 899–910. https://doi.org/10.1038/ni.3767.

72. Sidik, S.M., Hackett, C.G., Tran, F., Westwood, N.J., and Lourido, S. (2014). Efficient genome engineering of Toxoplasma gondii using CRISPR/Cas9. PLoS One *9*, e100450. https://doi.org/10.1371/journal.pone.0100450.

73. Shen, B., Brown, K.M., Lee, T.D., and Sibley, L.D. (2014). Efficient gene disruption in diverse strains of Toxoplasma gondii using CRISPR/CAS9. mBio *5*, e01114. https://doi.org/10.1128/mBio.01114-14.

74. Amos, B., Aurrecoechea, C., Barba, M., Barreto, A., Basenko, E.Y., Bażant, W., Belnap, R., Blevins, A.S., Böhme, U., Brestelli, J., et al. (2022). VEuPathDB: the eukaryotic pathogen, vector and host bioinformatics resource center. Nucleic Acids Res. *50*, D898–D911. https://doi.org/10.1093/nar/gkab929.

75. Sievers, F., Wilm, A., Dineen, D., Gibson, T.J., Karplus, K., Li, W., Lopez, R., McWilliam, H., Remmert, M., Söding, J., et al. (2011). Fast, scalable generation of high-quality protein multiple sequence alignments using Clustal Omega. Mol. Syst. Biol. *7*, 539. https://doi.org/10.1038/msb.2011.75.

76. Simossis, V.A., and Heringa, J. (2005). PRALINE: a multiple sequence alignment toolbox that integrates homology-extended and secondary structure information. Nucleic Acids Res. *33*, W289–W294. https://doi.org/10.1093/nar/gki390.

STAR★METHODS

KEY RESOURCES TABLE

REAGENT or RESOURCE	SOURCE	IDENTIFIER
Antibodies		
Mouse anti-HA.11	BioLegend	Cat#901514; RRID:AB_2565336
Mouse anti-FLAG	Sigma	Cat#F3165-5MG; RRID:AB_259529
Rabbit anti-HA	Proteintech	Cat#51064-2-AP; RRID:AB_11042321
Mouse anti-GRA2	Kindly provided by Dr. D. Soldati-Favre	NA
Mouse anti-GRA3	Kindly provided by Dr. D. Soldati-Favre	NA
Mouse anti-GRA5	BioVision	Cat#A1299
Rabbit anti-GRA7	Kindly provided by Dr. J. C. Boothroyd	NA
Rabbit anti-GRA17	This study	NA
Mouse anti-SAG1	GeneTex	Cat#GTX38936; RRID:AB_11164171
Chemicals, Peptides, and Recombinant Proteins		
Pyrimethamine	Sigma-Aldrich	Cat#P7771
Mycophenolic Acid	Sigma-Aldrich	Cat#M3536
Xanthine	Wako	Cat#245-00011
5-Fluoro-2′-deoxyuridine (FUDR)	Wako	Cat#067-01253
6-Thioxanthine	Wako	Cat#T385800
Critical Commercial Assays		
KOD FX *Neo*	TOYOBO	Cat#KFX-201
DNeasy Blood & Tissue Kit	Qiagen	Cat#69506
RNeasy Midi Kit	Qiagen	Cat#75144
Verso cDNA Synthesis Kit	Thermo Scientific	Cat#AB1453A
GoTaq qPCR and RT-qPCR Systems	Promega	Cat#A6001
Deposited Data		
CRISPR screen data	This study	GEO: GSE229545, GSE229547 and GSE229548
Experimental Models: Cell Lines		
Vero	This study	N/A
Mouse Embryonic Fibroblast (MEF)	This study	N/A
Experimental Models: Organisms/Strains		
T. gondii: Strain RH/Δhxgprt/Δku80	This study	N/A
T. gondii: Strain RH/Δhxgprt	This study	N/A
T. gondii: Strain RH/Δhxgprt/Δku80/ΔMIC19	This study	N/A
T. gondii: Strain RH/Δhxgprt/Δku80/ΔGRA50	This study	N/A
T. gondii: Strain RH/Δhxgprt/Δku80/ΔRON1	This study	N/A
T. gondii: Strain RH/Δhxgprt/Δku80/ΔGRA23	This study	N/A
T. gondii: Strain RH/Δhxgprt/Δku80/ΔROP18	This study	NA
T. gondii: Strain RH/Δhxgprt/Δku80/ΔRON11	This study	N/A
T. gondii: Strain RH/Δhxgprt/Δku80/ΔGRA72	This study	N/A
T. gondii: Strain RH/Δhxgprt/Δku80/ΔNAPE	This study	N/A

(*Continued on next page*)

Continued

REAGENT or RESOURCE	SOURCE	IDENTIFIER
T. gondii: Strain RH/Δhxgprt/Δku80/ΔTGGT1_203160	This study	N/A
T. gondii: Strain RH/Δhxgprt/Δku80/ΔGST2	This study	N/A
T. gondii: Strain RH/Δhxgprt/Δku80/ΔEPT1	This study	N/A
T. gondii: Strain RH/Δhxgprt/Δku80/ΔRAB4	This study	N/A
T. gondii: Strain RH/Δhxgprt/Δku80/ΔHMGB	This study	N/A
T. gondii: Strain RH/Δhxgprt/Δku80/ΔALG2	This study	N/A
T. gondii: Strain RH/Δhxgprt/Δku80/ΔDGAT1	This study	N/A
T. gondii: Strain RH/Δhxgprt/Δku80/ΔTGGT1_211695	This study	N/A
T. gondii: Strain RH/Δhxgprt/Δku80/ΔPDX1	This study	N/A
T. gondii: Strain RH/Δhxgprt/Δku80/ΔPDX2	This study	N/A
T. gondii: Strain RH/Δhxgprt/Δku80/ΔEF-P	This study	N/A
T. gondii: Strain RH/Δhxgprt/Δku80/ΔTGGT1_204350	This study	N/A
T. gondii: Strain RH/Δhxgprt/Δku80/ΔTGGT1_215890	This study	N/A
T. gondii: Strain RH/Δhxgprt/Δku80/ΔUSPase	This study	N/A
T. gondii: Strain RH/Δhxgprt/Δku80/ΔRad23	This study	N/A
T. gondii: Strain RH/Δhxgprt/Δku80/ΔHID1	This study	N/A
T. gondii: Strain RH/Δhxgprt/Δku80/ΔSui1	This study	N/A
T. gondii: Strain RH/Δhxgprt/Δku80/ΔGRA17	This study	N/A
T. gondii: Strain RH/Δhxgprt/Δku80/ΔGRA72+ GRA72-HA	This study	N/A
T. gondii: Strain RH/Δhxgprt/Δku80/ GRA23-HA	This study	N/A
T. gondii: Strain RH/Δhxgprt/Δku80/ΔGRA72/GRA23-HA	This study	N/A
T. gondii: Strain RH/Δhxgprt/Δku80/ΔUFM1	This study	N/A
T. gondii: Strain RH/Δhxgprt/Δku80/ΔUFM1+UFM1(WT)	This study	N/A
T. gondii: Strain RH/Δhxgprt/Δku80/ΔUFM1+UFM1(G87A)	This study	N/A
C57BL/6 mice	SLC	N/A
Ifngr1$^{-/-}$mice	Sasai et al.[71]	N/A
Oligonucleotides		
For primers and oligonucleotides, see Table S4	This study	N/A
Recombinant DNA		
For each gRNA sublibrary, see Tables S1–S3	This study	N/A
pU6-Universal	Sidik et al.[72]	Addgene plasmid: #52694
pSAG1-GRA72-HA-HXGPRT	This study	N/A
pUPRT-UFM1(WT)	This study	N/A
pUPRT-UFM1(G87A)	This study	N/A

(*Continued on next page*)

Continued

REAGENT or RESOURCE	SOURCE	IDENTIFIER
Software and Algorithms		
R v4.1.1	R Foundation for Statistical Computing	https://www.r-project.org/
RStudio	posit	https://posit.co/products/open-source/rstudio/
Prism9	GraphPad	https://www.graphpad.com/

RESOURCE AVAILABILITY

Lead contact

Further information and requests for resources and reagents should be directed to and will be fulfilled by the lead contact, Masahiro Yamamoto (myamamoto@biken.osaka-u.ac.jp).

Materials availability

Toxoplasma gondii transgenic strains and unique reagents generated in this study are available upon request from the lead contact.

Data and code availability

- The CRISPR screen data of three sublibraries have been deposited to the NCBI GEO. The GEO accession numbers are GSE229545, GSE229547 and GSE229548.
- This paper does not report original code.
- Any additional information required to reanalyze the data reported in this paper is available from the lead contact upon request.

EXPERIMENTAL MODEL AND SUBJECT DETAILS

Toxoplasma strains

RHΔhxgprt, RHΔhxgprtΔku80 and its derivatives of *Toxoplasma* were maintained in Vero cells and passaged every 3 days using RPMI (Nacalai Tesque) supplemented with 2% heat-inactivated fetal bovine serum (FBS; JRH Bioscience), 100 U/ml penicillin and 0.1 mg/mL streptomycin (Nacalai Tesque) in incubators at 37°C and 5% CO_2.

Host cell culture

Vero cells were maintained in RPMI (Nacalai Tesque) supplemented with 10% heat-inactivated FBS, 100 U/ml penicillin and 0.1 mg/mL streptomycin (Nacalai Tesque) in incubators at 37°C and 5% CO_2. Mouse embryonic fibroblasts (MEFs) were maintained in DMEM (Nacalai Tesque) supplemented with 10% heat-inactivated FBS, 100 U/ml penicillin and 0.1 mg/mL streptomycin (Nacalai Tesque) in incubators at 37°C and 5% CO_2.

Mice

C57BL/6NCrSlc (C57BL/6N) mice were purchased from SLC. *Ifngr1*$^{-/-}$ mice were previously generated and described.[71] All experiments were conducted in 8-10-week-old female mice. All animal experiments were conducted with the approval of the Animal Research Committee of Research Institute for Microbial Diseases in Osaka University.

METHOD DETAILS

Plasmid construction for knockout *Toxoplasma*

For construction of the CRISPR/Cas9 plasmids for targeting a gene of interest (GOI), two oligonucleotide primers (GOI_gRNA1_F and GOI_gRNA1_R, GOI_gRNA2_F and GOI _gRNA2_R) containing gRNA sequence were annealed and cloned into BsaI site of the pU6-Universal vector (Addgene #52694). To generate a construct for deleting the entire coding region of GOI, flanking regions of 60 bp of 5′ AND-3′ outside the gRNAs were used to surround the genes. Forward and reverse primers with homology to the floxed HXGPRT cassette and to the 5′ AND-3′ coding sequence of the GOI was used (GOI_targeting_F and GOI_targeting_R). The targeting strategy and primer sequences used for the genetic disruption are shown in Figure S2A and Table S4A, respectively.

Generation of gene knockout *Toxoplasma*

RHΔhxgprtΔku80 were filtered and resuspended in Cytomix (10mM KPO_4, 120mM KCl, 0.15 mM $CaCl_2$, 5mM $MgCl_2$, 25 mM HEPES, 2 mM EDTA). Parasites were mixed with 50 μg of each gRNA1 and gRNA2 CRISPR plasmids with the PCR-amplified targeting fragment for each GOI, and supplemented with 2 mM ATP, 5mM GSH. Parasites were electroporated by GENE PULSER II (Bio-Rad

Laboratories). Transfected parasites were selected by 25 μg/mL mycophenolic acid (MPA) (Sigma) and 50 μg/mL Xanthine (Wako) to obtain stably resistant clones. Then, parasites were subjected to limiting dilution in 96-well plates to isolate single clones. To confirm the disruption of the gene, we analyzed the mRNA expression by quantitative RT-PCR.

Complementation of GRA72 and UFM1

To complement the ΔGRA72 parasites, GRA72 cDNA was generated by PCR amplification from cDNA of the RH strain. The PCR products were inserted into pBlueScript plasmid vector, in which 1 kb promoter of the *SAG1* gene was fused to GRA72 cDNA and followed by HA tag, the polyA sequence and HXGPRT expression cassette. The *hxgprt* cassette which is inserted in the endogenous GRA72 locus of ΔGRA72 parasites was deleted with Cre transfection and selected in the presence of 6-thioxanthine (6-TX). ΔGRA72Δhxgprt parasites were transfected with GRA72-HA complementation vector and selected in the presence of MPA/Xanthine and subjected to limiting dilution.[45] Isolated clones were examined for GRA72-HA protein expression by western blotting.

To complement the ΔUFM1 parasites, FLAG-UFM1 (WT) or the mutant FLAG-UFM1(G87A) cDNA were generated by PCR amplification from cDNA of the RH strain. The pUPRT vectors were generated in which FLAG-UFM1(WT) or FLAG-UFM1(G87A) were expressed from the endogenous UPRT promotor. ΔUFM1 parasites were transfected with this pUPRT vector and gRNA targeting UPRT and selected by FUDR (Wako).[73] Parasites were subjected to limiting dilution and isolated clones were examined for FLAG-UFM1 protein expression by western blotting. The correct UFM1 sequences of isolated clones were checked by Sanger sequencing by 3130xl genetic analyzer (Applied Biosystems). The primer sequences used for gene complementation are listed in Table S4B.

Generation of custom anti-GRA17 antibody

Custom anti-GRA17 antibody (rabbit polyclonal) was generated against a synthetic C-terminal peptide of GRA17 (KMAVKQKAMQGKQ). The epitope identification, peptide synthesis, rabbit immunization and serum collection were conducted by Cosmo Bio. The specificity of anti-GRA17 antibody was validated for western blotting and IFA (Figures S5D and S5E)

Immunofluorescence assay

MEFs were cultured on glass coverslips, infected with *Toxoplasma* for 24–48 h, and fixed in PBS containing 3.7% paraformaldehyde for 10 min at room temperature. Cells were permeabilized with PBS containing 0.002% Digitonin for 5 min and then blocked with 8% FBS containing PBS for 1 h at room temperature. Then, the coverslips were incubated with the primary antibodies for 1 h, followed by incubation with Alexa Fluor 488-, Alexa Fluor 594-conjugated secondary antibodies and DAPI for 30 min. The coverslips were mounted using PermaFluor (Thermo Scientific). Images were acquired by confocal laser microscopy (Olympus FV3000 IX83).

Assessment of *in vivo* virulence in mice

Mice were infected with 1000 tachyzoites in 200 μL (intra-peritoneum) or 40 μL (intra-footpad) PBS. Parasite viability was determined by plaque assay. The mouse health condition and survival were monitored daily until 30 days (intra-peritoneum) or 40 days (intra-footpad) post infection, respectively.

Quantitative RT-PCR

Total RNA was extracted by RNeasy kit (QIAGEN), and cDNA was synthesized by Verso reverse transcription (Thermo Fisher Scientific) according to the manufacturer's instructions. Quantitative RT-PCR was performed with a CFX Connect real-time PCR system (Bio-Rad Laboratories) and a Go-Taq real-time PCR system (Promega). The data were analyzed by the ΔΔCT method and normalized to ACT1 in each sample. The primer sequences are listed in Table S4C.

Western blotting

Cells were lysed in lysis buffer (1% NP-40, 150 mM NaCl, 20 mM Tris-HCl, pH 7.5) containing a protease inhibitor cocktail (Nacalai Tesque). The cell lysates were separated by SDS-PAGE and transferred to polyvinylidene difluoride membranes (Immobilon-P; Millipore) and subjected to western blotting using the indicated antibodies as described previously.[45] SAG1 was used as the parasite loading control.

Endogenous GRA23 tagging at the C terminus

The fragments containing HA epitope flanked by homology regions to the C terminus of GRA23 were PCR-amplified (GRA23-HA_tagging_F and GRA23-HA_tagging_R) (Table S4B) and co-transfected with 50 μg of pU6-Universal carrying gRNA.[72] Transfected parasites were cultured until their first lysis and used to infect MEF monolayers grown on coverslips. Localization of the HA-tagged GRA23 was determined 24 h post infection by IFA.

In vitro and *in vivo* pooled CRISPR screens

The gRNA sequences of the rhoptry/DG sublibrary, the endomembrane-nucleus sulibrary and the metabolism sublibrary were selected from the genome-wide gRNA library.[36] In addition, we designed new gRNAs for some ROP/GRA genes such as ROP5 and ROP7, since they are excluded from the original genome-wide gRNA library. The selected gRNA sequences were cloned into

the modified pU6-Universal vector by cloning a T2A, DHFR drug selection marker, T2A and RFP in frame with Cas9, where the expression of gRNA and Cas9-T2A-DHFR-T2A-RFP cassettes was independently transcribed. The Cas9(C terminus)-T2A-DHFR-T2A-RFP cassette was artificially synthesized by FASMAC. The insertion of the selected gRNA sequences into the modified pU6-Universal vector was outsourced and performed by VectorBuilder. The gRNA library (200 μg) was linearized with NotI and transfected into approximately 1–2×10^8 RHΔhxgprt parasites divided between four separate cuvettes. Then, transfected parasites were grown in 4 × 150-mm dishes with confluent Vero cell monolayers and pyrimethamine (Sigma) was added 24 h later. All the parasites were passaged every 3 days until Passage 3 (P3) without filtration. After 2 days (Passage 4), the parasites were syringe lysed, filtered and counted for genomic DNA preparation or for mouse infection. For genomic DNA preparation, at least 1×10^8 parasites were pelleted and stored at −80°C. For mouse infection, the parasites were resuspended in PBS at a concentration of 2.5×10^8 parasites/ml. Then, 1×10^7 parasites in 40 μL PBS were infected into footpad of each WT or *Ifngr1*$^{-/-}$ mouse. Parasite viability was determined by plaque assay. At 7 days post infection, the spleens were collected and crushed by a plunger and passed through a cell strainer to make single cell suspensions. Then, the suspensions were pelleted and added to 2 × 150-mm dishes per spleen with confluent Vero cell monolayers. After 2–4 days, when the parasites completely lysed out, they were filtered and counted. At least 1×10^8 parasites were pelleted and stored at −80°C. Parasite genomic DNA was extracted using the DNeasy Blood and Tissue kit (Qiagen) and integrated gRNA sequences were amplified and barcoded by PCR (Primer 1 and Primer 2) with KOD FX *Neo* (TOYOBO) (Tables S4D and S4E). Genomic DNA (1μg) was used for the template. The resulting libraries were sequenced on a DNBSEQ-G400RS (MGI) using Primer 3 and Primer 4 (Table S4D).

Bioinformatic analysis of the CRISPR screen

Following demultiplexing, gRNA sequencing reads were aligned to the gRNA library. The abundance of each gRNA was calculated and normalized to the total number of aligned reads. For *in vitro* analysis, the log2 fold-change between the P4 sample and the library was calculated for each gRNA. The fitness score for each gene was calculated as the mean log2 fold change for the top five scoring guides. For *in vivo* analysis, the log2 fold-change between each *in vivo* sample and the P4 sample was calculated for each gRNA as described above. The median fitness score across mouse replicates was used as the *in vivo* fitness score. For a given gene, gRNAs were compared using Wilcoxon rank-sum test between P4 vs. WT mice or WT mice vs. *Ifngr1*$^{-/-}$ mice. The p values for each test were adjusted using the Benjamini-Hochberg method. Hierarchical clustering and primary component analysis were conducted on the mean *in vivo* fitness scores for each gene (Table S1D). Ward's method was applied for hierarchical clustering. The distance of each gene from the regression line was calculated as below.

$$\boldsymbol{distance}(\boldsymbol{ax} + \boldsymbol{by} + \boldsymbol{c} = \boldsymbol{0}, (\boldsymbol{x_0}, \boldsymbol{y_0})) = \frac{\boldsymbol{ax_0} + \boldsymbol{b}\,\boldsymbol{y_0} + \boldsymbol{c}}{\sqrt{\boldsymbol{a^2} + \boldsymbol{b^2}}}$$

All analyses were conducted by R (v4.1.1) with package stats (v3.6.2) and visualized by ggplot2 (v3.4.0).

GRA72 and UFM1 phylogenetic analysis

VEuPathDB and BLAST were searched for *Toxoplasma* GRA72 or UFM1 homologues.[74] Clustal Omega and PRALINE were used to align and visualize obtained homologues.[75,76]

QUANTIFICATION AND STATISTICAL ANALYSIS

Information about the number of biological replicates and the type of statistical tests used can be found in the figure legends. All statistical analyses except for the survival rates were performed using R (4.1.1, https://www.r-project.org/). For correlation analysis, Pearson's correlation was used. Data with p values <0.05 were considered statistically significant. The statistical analysis of survival rates was performed by the log rank test using the GraphPad Prism9 software.